

Jovian Dust: Streams, Clouds and Rings

Harald Krüger

Max-Planck-Institut für Kernphysik, Heidelberg

Mihály Horányi

LASP and Department of Physics, University of Colorado

Alexander V. Krivov

Institut für Physik, Universität Potsdam

Amara L. Graps

Max-Planck-Institut für Kernphysik, Heidelberg

1 INTRODUCTION

Dust is both a messenger of and participant in cosmic processes. Like photons, a dust particle is born at remote sites in space and time and carries information on its formation and history. Dust particles are dispersed in space by gravitation, magnetic and radiation fields and, therefore, act as astrophysical tracers, responding to their environment as well as altering their environment. We can infer properties about a dust's past and present environment from the particle's physical properties and its chemical composition.

In the dust evolution cycle, dust offers a tangible, physical link between our planetary system and the stars. For example, it is an intimate player in proto-planetary accretion disks and the formation of planetesimals. Therefore, the study of dust in space can provide important information on the fundamental processes governing the formation of planetary systems. The dust in a planetary system is the most processed of the different populations of cosmic dust. It is replenished by sources such as dust from asteroid collisions, cometary activity and collisions in the inner solar system and in the outer regions like the Kuiper Belt. These dust populations can impressively display their presence as cometary dust tails and the zodiacal light. The dust environment is denser in the vicinity of planets where the dust is produced by endogenic and exogenic processes associated with satellites, collisions in dense rings, and dust can also be captured from interplanetary space by planetary magnetospheres. However, our knowledge of dust in a planetary environment – apart from the Earth – was relatively sparse before the *Galileo* mission to Jupiter.

The subject of this chapter is dust in the environment of Jupiter. By the term “dust” we mean solid particulates whose typical sizes range from several nanometers up to several microns. Until the mid 1970s, dust had been studied extensively in interplanetary space (Fechtig *et al.* 2001) but its presence in the environment of Jupiter was pure speculation. The first indications that dust exists in the jovian

system came from the *Pioneer 10* and *11* spacecraft, which passed by the planet in 1973 and 1974, respectively. During their passage through the jovian system, the in situ dust detectors on board both spacecraft recorded several impacts of dust particles (Humes *et al.* 1974). Even these few impacts represented a flux which was, by three orders of magnitude, larger than the dust flux measured in interplanetary space. These measurements proved the existence of dust in the jovian environment. The penetration detectors used at the time, however, could only detect particles larger than several microns.

In 1979, the two *Voyager* spacecraft drastically changed our picture of jovian dust, even though they were not equipped with dedicated dust detectors: Jupiter's dusty rings were discovered on images from the *Voyager* cameras, although earlier hints that this faint dusty ring might exist came from a dip in the density of charged particles measured near *Pioneer 11*'s closest approach to Jupiter (Filius *et al.* 1975, Acuña and Ness 1976), as well as from the impact events recorded by the *Pioneer* dust detectors. Another discovery by *Voyager*, which had a large influence on later dust research, was active volcanism on Io. At the time, there were conjectures that tiny dust grains entrained in Io's plumes might be ejected into circumjovian space by electromagnetic forces (Johnson *et al.* 1980, Morfill *et al.* 1980).

The next major step forward in the investigation of dust in the jovian system came from the Jupiter flyby of the *Ulysses* spacecraft in 1992. The impact ionization dust detector of *Ulysses* is five orders of magnitude more sensitive (of particle mass) than the *Pioneer 10/11* detectors (Grün *et al.* 1992b). Within 2 AU from the planet, *Ulysses* discovered intermittent collimated streams of dust particles. The streams occurred at approximately monthly intervals (28 ± 3 days) and the maximum impact rates exceeded, by three orders of magnitude, the rates typically measured in interplanetary space (Grün *et al.* 1993, Baguhl *et al.* 1993); Figure 10.1. These fluctuations were a complete surprise

Table 10.1. Physical parameters of dust populations (1) studied in situ at Jupiter, (2) gives typical particle sizes (radii) assuming spherical particles, (3) are average measured impact speeds, (4) lists the radial distance range where the particles have been detected and (5) and (6) give the derived particle number densities and mass densities in space, respectively. Each dust population is discussed in the section listed in (7).

Population (1)	Particle Size (μm) (2)	Impact Speed (km s^{-1}) (3)	Jovicentric Distance (4)	Number Density (m^{-3}) (5)	Mass Density (kg m^{-3}) (6)	Section (7)
Stream particles	$\sim 0.01^*$	$\sim 300^*$	$6 R_J - 2 \text{ AU}$	$10^{-3} - 10^{-8}$	$10^{-23} - 10^{-28}$	10.3/10.4
Ejecta clouds	0.3–1	6–8	$\leq 10 R_{\text{sat}}^\dagger$	$10^{-4} - 10^{-5}$	$10^{-19} - 10^{-20}$	10.5
Ejecta ring	0.6–2	~ 7	$6 - 30 R_J$	$10^{-6} - 10^{-7}$	$10^{-20} - 10^{-21}$	10.6
Captured particles	0.5–1.5	~ 20	$6 - 20 R_J$	$\sim 10^{-7}$	$\sim 10^{-21}$	10.6
Outskirts ring	1–2	~ 5	$\geq 50 R_J$	$\sim 10^{-8}$	$\sim 10^{-22}$	10.6

*: derived from dynamical modeling

†: altitude above satellite surface

because no periodic phenomenon for small dust particles in interplanetary space was known before. The measured impact directions implied that the particles interacted with the interplanetary magnetic field, and that they originated from the jovian system. Jupiter's magnetosphere was recognised as the ultimate source of these high-velocity dust particles, provided that they could collect a positive electrical charge, and hence gain energy from the outward pointing corotational electric field. The source, however, could not be derived from the *Ulysses* measurements alone. From modeling the particle dynamics, Io (Horányi et al. 1993a, Maravilla et al. 1995) and Jupiter's gossamer ring (Hamilton and Burns 1993) were suggested as the most likely sources of the jovian dust streams.

The jovian dust streams were confirmed in 1995, when the *Galileo* spacecraft approached Jupiter (Grün et al. 1996a, Krüger et al. 1999b). *Galileo* is equipped with a twin of the *Ulysses* dust detector (Grün et al. 1992a). Modeling of the particles' dynamics led to grain sizes of about 10 nm and impact speeds exceeding 200 km s^{-1} Zook et al. (1996). (See Grün et al. (2001) for a comprehensive review of 10 years of *Ulysses* dust measurements.)

During its seven-year orbital tour about Jupiter, *Galileo* has provided the first opportunity for long-term in situ dust studies in the environment of a giant planet. Apart from the jovian dust streams, *Galileo* allowed for studies of impact-generated dust clouds surrounding the Galilean satellites (Krüger et al. 1999e), a tenuous dust ring in the region between the Galilean satellites (Thiessenhusen et al. 2000, Krivov et al. 2002a) and further out from the satellites (Krivov et al. 2002b), as well as interplanetary and interstellar particles captured by the jovian magnetosphere (Colwell et al. 1998b,a). At the end of 2000, the flyby of the *Cassini* spacecraft at Jupiter offered the unique opportunity for in situ dust measurements with two spacecraft at Jupiter. The dust analyser on board *Cassini* is an upgrade of the *Galileo* and *Ulysses* instruments. With five dedicated dust detectors flown on Jupiter-passing spacecraft, the dust environment of Jupiter has been studied as extensively as has the natural cosmic dust environment around the Earth.

Unlike larger jovian bodies, the dynamics of dust in the jovian system is strongly affected by electrodynamic forces. Like all astronomical bodies, particles in the jovian system are exposed to plasmas and UV radiation and collect elec-

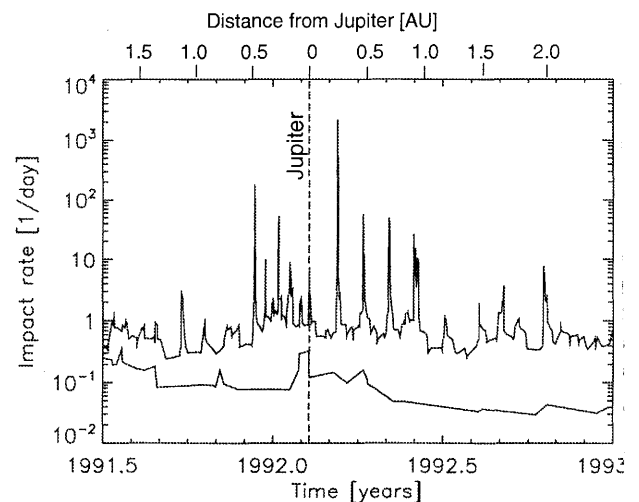


Figure 10.1. Impact rate of dust particles observed with *Ulysses* during its Jupiter flyby (dashed vertical line). The curves show impacts recorded (upper curve) and impacts of dust particles with masses greater than 10^{-15} kg (lower curve). The impact rates are a sliding average over six impacts. The distance from Jupiter indicated at the top. Note that after Jupiter flyby the spacecraft receded from the planet at about 35° jovigraphic latitude (Grün et al. 2001).

trostatic charges. However, if the dust particles are small enough, their dynamics can be dominated by electric and magnetic forces. For micron-sized and smaller dust grain magnetospheric effects can shape the particles' size and spatial distributions. The ring/halo region, the dust stream, the captured ring at Jupiter and the ring supplied by ejecta from the Galilean satellites are recent examples where dust plasma interaction effects can best explain the observations. In this chapter, we describe measurements of the different populations of jovian dust and provide plausible gravitational and electrodynamic explanations for the dust's dynamics. The properties of the individual dust populations are summarized in Table 10.1.

We mainly confine this chapter to dust outside of Io's orbit, where most of the presently available in situ dust data have been collected. For dust within Io's orbit—especially the jovian ring system—the reader is referred to Chapte

Additional information about the in situ dust measurements in the jovian system can be found at <http://www.mpi-mpg.de/dustgroup/>.

2 IN SITU DUST DETECTION

Most of the measurements discussed in this chapter have been obtained with the *Galileo* dust detector (DDS), describe this instrument in some detail before we discuss the jovian dust environment.

Galileo is a dual-spinning spacecraft with an antenna (negative spin axis direction) that usually points towards Earth. The dust detector (Figure 10.2) is mounted on the spinning section of the spacecraft and the sensor axis is offset by 60° from the positive spin axis (i.e., usually the anti-Earth direction). The geometry of dust detection is sketched in Figure 10.2. The field of view (FOV) of the dust detector is a cone of 140° full angle. The sensor area for impacts depends on the angle between the impact direction and the spin axis. The maximum sensitive area of the detector averaged over one spacecraft revolution is 235 cm^2 (Krüger *et al.* 1993c). The impact direction (rotation angle, *ROT*) is determined from the spin position of the spacecraft around its spin axis at the time of a dust impact. The rotation angle $ROT = 0^\circ$ corresponds to a dust sensor axis orientation closest to the ecliptic north direction. The rotation angle measured in a right-handed system around the antenna direction.

The *Galileo* dust detector (Grün *et al.* 1992a) is an impact ionization sensor, that measures the plasma cloud generated upon impact of sub-micron- and micron-sized dust particles on to the detector target. Up to three independent measurements of the ionization cloud created during impact are used to derive both the mass and the impact speed of the dust grains (Grün *et al.* 1995c). The detector mass threshold, m_t , is proportional to the positive charge component, Q_+ , of the plasma produced during the impact, which, itself, only depends on the impact speed, w . Using the calibration parameters $(Q_+/m)_0$, m_0 , w_0 , and α , which have been determined from detector calibrations (Grün *et al.* 1995c), the corresponding mass threshold is:

$$m_t = \frac{Q_+}{(Q_+/m)_0} = m_0 \left(\frac{w_0}{w} \right)^\alpha \quad (10.1)$$

with exponent $\alpha \sim 3.5$. For example, an impact charge of $Q_+ = 8 \times 10^{-14} \text{ C}$ refers to a mass threshold $m_t = 3 \times 10^{-17} \text{ kg}$ at 20 km s^{-1} impact speed.

The dynamic range of the impact charge measurement is 10^6 , which is also the dynamic range of the mass determination for particles with constant impact speeds. The calibrated speed range of the instrument is $2 \text{ km s}^{-1} \leq w \leq 20 \text{ km s}^{-1}$, which corresponds to a calibrated mass range of 10^{-19} to 10^{-9} kg . Impact speeds can be determined with an accuracy of about a factor two and the accuracy of the mass determination of a single particle is about a factor of ten. Impact rates are derived from the number of detections within a given time interval.

The *Ulysses* spacecraft carries a dust detector which is nearly identical to *Galileo*'s dust detector. Dust data obtained with the detectors on board both spacecraft—*Ulysses* and *Galileo*—can be found in the literature (Grün *et al.*

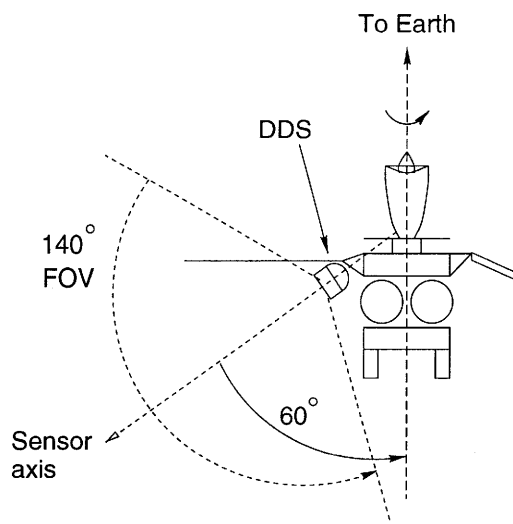


Figure 10.2. Schematic configuration of the *Galileo* dust detector (DDS): the antenna (top) points towards Earth and the dust detector (DDS) largely faces the anti-Earth hemisphere. The sensor axis has an angle of 60° from the positive spin axis (i.e., the anti-Earth direction). During one revolution of the spacecraft the sensor axis scans a cone with 120° opening angle. The 140° wide FOV of DDS is indicated by dotted lines. The sensor orientation shown corresponds to a rotation angle of 270° if viewed from the north ecliptic pole.

1995a,b, Krüger *et al.* 1999d,c, 2001a,b). The *Cassini* dust instrument is an upgrade of the *Galileo* and *Ulysses* detectors. It is, by an order of magnitude, more sensitive in impact charge, and can also measure the chemical composition of dust particles (Srama *et al.* 2004).

10.3 JOVIAN DUST STREAM MEASUREMENTS

The jovian dust streams detected with *Ulysses* during its approach to Jupiter in 1992 demonstrated the interaction of charged dust particles with a planetary magnetosphere for the first time. In this section we discuss the measurements of the dust streams obtained mostly within Jupiter's magnetosphere and in Section 10.4 we present a numerical model for their dynamics.

10.3.1 Electromagnetically Interacting Dust

The impact directions of the dust stream particles measured with *Galileo* and *Ulysses* in interplanetary space were close to the line-of-sight direction to Jupiter. The approach direction of most streams, however, deviated too much from the direction to Jupiter to be explained by gravitational forces alone. This deviation was correlated with the magnitude and the direction of the interplanetary magnetic field (Grün *et al.* 1996a), which implied that strong non-gravitational forces must have been acting on the grains. The observed 28-day period in the impact rate (Figure 10.1) was most likely caused by changes in the tangential component of the solar wind magnetic field, which periodically accelerated the particles towards and away from the ecliptic plane (Hamilton and Burns 1993). Numerical simulations have shown that

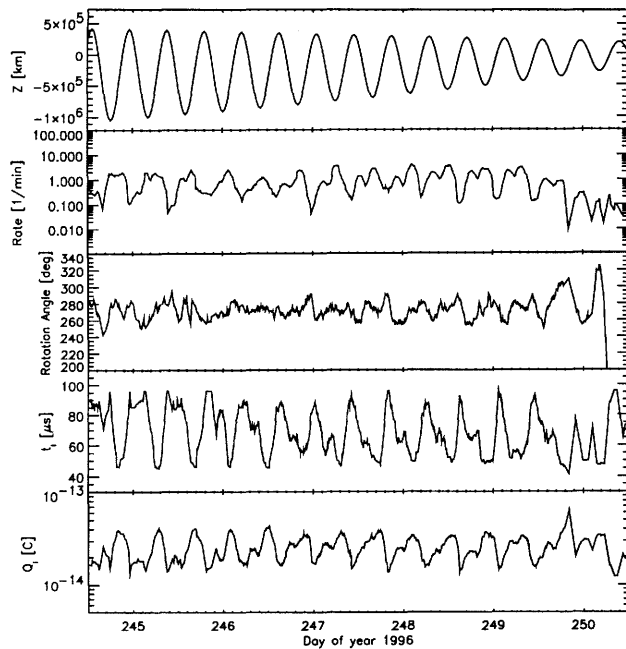


Figure 10.3. Phase relation between *Galileo*'s position in Jupiter's magnetic field (here *Galileo*'s distance from the magnetic equatorial plane, Z) and observed impact rate, impact direction (rotation angle), ion charge rise time t_1 and ion charge amplitude Q_1 during part of *Galileo*'s G2 orbit about Jupiter in 1996 (Grün *et al.* 1998). A dipole tilted at 9.6° with respect to Jupiter's rotation axis pointing toward $\lambda_{\text{III}} = 202^\circ$ has been adopted for the magnetic field. The observed data have been smoothed with a 2 hr average. In the time interval shown, the spacecraft approached Jupiter from $60 R_J$ to $10 R_J$ joviocentric distance (Jupiter radius, $R_J = 71\,492$ km).

only particles with velocities in excess of 200 km s^{-1} and radii a in the range $5 \text{ nm} \leq a \leq 15 \text{ nm}$ are compatible with the observations (Zook *et al.* 1996) (It should be noted that these speeds are well beyond the calibrated range of DDS). Larger (smaller) grains do not interact enough (interact too strongly) with the interplanetary magnetic field to explain the observed impact directions. This demonstrates that the solar wind magnetic field acts as a giant mass-velocity spectrometer for charged dust grains.

Strong electromagnetic interactions of dust grains have also been studied with the *Galileo* detector within the jovian magnetosphere. These grains are the continuation of the dust streams measured with *Ulysses* and *Galileo* in interplanetary space. Figure 10.3 shows an example of impact parameters measured while *Galileo* was in the inner part of the magnetosphere. During this and most other times when *Galileo* has collected data in this spatial region, the impact rate fluctuated with 5- and 10-hr periods and the fluctuations typically reached two orders of magnitude. Furthermore, the impact directions of the grains and the measured charge rise times and charge amplitudes, which are used to derive particle speeds and masses, show similar fluctuations (Grün *et al.* 1998). These fluctuations are correlated with the position of *Galileo* in the jovian magnetic field (upper panel in Figure 10.3). Due to a 9.6° tilt of Jupiter's magnetic axis with respect to the planet's rotation axis, the magnetic

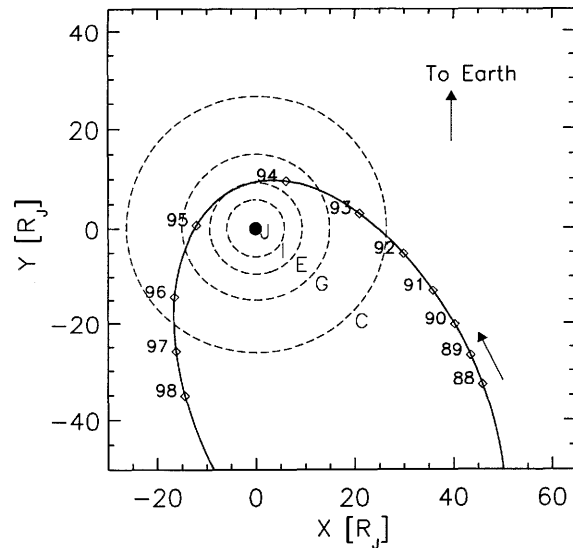


Figure 10.4. *Galileo*'s orbit trajectory during the G7 flyby Ganymede projected on to Jupiter's (J) equatorial plane (Jup. radius, $R_J = 71\,492$ km). The orbits of the Galilean satellites are shown: Io (I), Europa (E), Ganymede (G), and Callisto (C). Days are marked by diamonds (numbers give day of year in 1997). *Galileo*'s path through the jovian system. Earth direction is the top.

equator sweeps over the spacecraft in either up- or downward direction every 5 hr, causing the fluctuations in the measured impact parameters.

A highly time-resolved example of the measured impact rate of our smallest dust impacts ($Q_1 < 10^{-13}$ C) from *Galileo*'s G7 orbit about Jupiter is shown in the upper panel of Figure 10.5 (the G7 orbit is sketched in Figure 10.4). When *Galileo* approached Jupiter, the impact rate increased to values exceeding 10 min^{-1} (Days 91 and 93). Around perijove passage, the impact rate dropped to about 0.1 min^{-1} . Between Day 88 and Day 94, the impact rate fluctuated more than an order of magnitude, with periods of about 5 and 10 hr. At Ganymede closest approach, a sharp peak occurred which lasted only several minutes (these impacts will be discussed in Section 10.5). Interestingly, the impact rate shows three broad maxima (Days 89, 91 and 93) which are about two days apart (see also Section 10.3.3).

10.3.2 Impact Directions

An example of the measured impact directions (rotation angles) of the dust particles, as derived from the sensor orientation at the time of particle impact, is shown in the bottom panel of Figure 10.5. The impact direction of a single particle is only known to lie somewhere within the 140° -wide FOV. The average of all the rotation angle arrival directions of dust particles belonging to a stream is known with much higher accuracy than is the impact direction of a single particle.

When *Galileo* was approaching Jupiter, the dust impact direction was concentrated between 210° and 330° . No stream particles were detected before Day 87. Half a day before perijove passage, the impact direction of the stream particles shifted by 180° , and they approached from

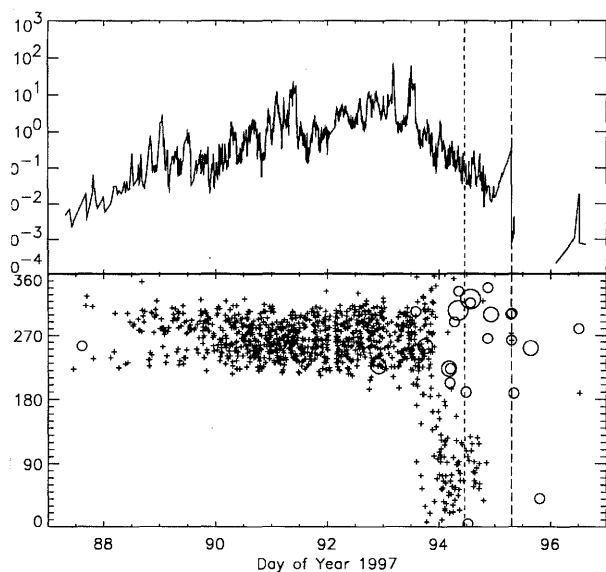


Figure 10.5. Dust data from *Galileo*'s G7 orbit (28 March to April 1997). Upper panel: Impact rate of small dust particles (impact charge $Q_I < 10^{-13}$ C). Lower panel: Sensor direction time of dust particle impact (rotation angle) for those impacts for which the complete information has been transmitted Earth (Krüger *et al.* 2001a). Small particles (impact charge $< 10^{-13}$ C) are shown as crosses, bigger particles are shown as circles. The size of the circles indicates the impact charge $-13 \text{ C} \leq Q_I \leq 10^{-10} \text{ C}$. At 0° the sensor points close to the geographic north direction, at 90° and 270° the sensor points close to Jupiter's equatorial plane. The closest approach to Ganymede on 5 April 1997 is indicated by a dashed line and perijove passage by a dotted line. On Day 88, *Galileo* was at a joviocentric distance of about $50 R_J$, perijove distance was at $9.1 R_J$ (Krüger *et al.* 1999a).

in opposite direction. This change in impact direction is consistent with the drop in the impact rate at Day 94.0

(Figure 10.5, upper panel). At Day 94.8 impacts of all stream particles ceased. The times of onset, shift by 90° and cessation of dust impacts give important information about the particle's dynamics. These times can best be explained by tiny electromagnetically-interacting dust particles with radii of about 10 nm (Section 10.4.3). The vast majority of the particles were small sub-micron-sized dust particles, which just exceeded the detection threshold ($10^{-14} \text{ C} \leq Q_I \leq 10^{-13} \text{ C}$; crosses). Only about 20 bigger particles ($10^{-13} \text{ C} \leq Q_I \leq 10^{-11} \text{ C}$ filled circles) were detected within two days around perijove passage, i.e., within $1 R_J$ from Jupiter, and they belong to a tenuous dust ring surrounding the region between the Galilean satellites (this dust ring is discussed in Section 10.6). Four of these impacts occurred within 1 hr of closest approach to Ganymede. They are particles belonging to a steady-state dust cloud surrounding this jovian moon (discussed in Section 10.5).

The rotation angle distribution on Days 88 and 89 shows an interesting void between 250° and 280° ; fewer particles are detected in this range in rotation angles than in the range of larger and smaller angles. This gap is due to a shading of the dust detector by *Galileo*'s magnetometer boom, as well as by the Energetic Particles Detector (EPD, Williams *et al.* 1992) and the Plasma Subsystem (PLS, Frank *et al.*

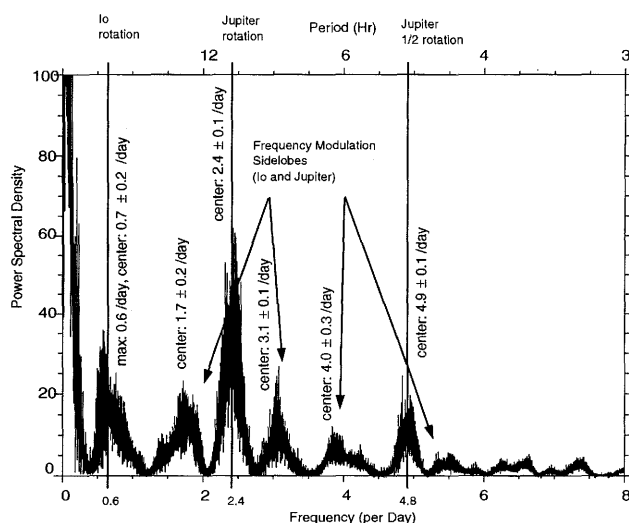


Figure 10.6. A Scargle-Lomb periodogram (Scargle 1982) for two years (1996 and 1997) of *Galileo* dust data; (from Graps *et al.* (2000)). A carrier source (Io) is modulated by Jupiter's magnetic field frequency which leads to "modulation product" peaks at 13.9 and 7.7 hr. There are additional frequencies: a half period of Jupiter's magnetic field (4.9 hr), Io as a single source (41.9 hr), and a low-frequency oscillation trend due to the spacecraft orbital geometry (Graps *et al.* 2000).

1992) instruments which are mounted to the magnetometer boom (Kivelson *et al.* 1992) of *Galileo*. The boom is in the field of view of the dust instrument for particles approaching the sensor at angles more than 30° away from the positive spin axis (cf. inset of Figure 10.4). This shading by the boom and the shape of the rotation angle distribution imply that the dust streams are collimated to within a few degrees (Krüger *et al.* 1999c).

Particles detected within about an hour of Ganymede's closest approach came from the direction between 250° and 310° . Note that the dust streams had already vanished half a day earlier (see also Section 10.5).

10.3.3 Io's Frequency Signature

In Section 10.3.1 we presented strong evidence for the electrodynamic interaction of the jovian dust stream particles with the planet's magnetosphere: 5- and 10-hr fluctuations of the impact rate are compatible with Jupiter's rotation period.

In addition to the 5- and 10-hr periods, a modulation of the dust impact rate with Io's orbital period (42 hr) could also be recognized during some time intervals (e.g., for *Galileo* orbits E4, G7 and C9 see Grün *et al.* 1998, Krüger *et al.* 1999a,c, respectively) while at other times an Io modulation was missing (e.g., orbit G2, Figure 10.3). A detailed frequency analysis of a two-year data set shows Io's orbital frequency as a "carrier frequency" and primary source of the jovian dust streams (Figure 10.6, Graps *et al.* 2000). Jupiter's magnetic field frequency modulates Io's frequency signal, giving rise to modulation side lobe products seen around first order (10 hr) and harmonic (5 hr) Jupiter magnetic field frequencies. These modulation products confirm Io's role as a primary source of the jovian dust streams. Io

as a source can best explain the time series analysis results showing Io's orbit periodicity. The periodogram peaks give a rough estimate of the fraction of dust from Io: if we sum under the Io peak and the modulation side lobes (primary and first harmonic), that fraction amounts to 60% of the total mass. The remaining mass fraction can come from Io or elsewhere, but it has lost Io's frequency signature. An Io source is also compatible with the deduced particle sizes of $a \sim 10$ nm: photometric observations of the Io plumes obtained with *Voyager* imply a size range of 5 to 15 nm (Collins 1981), in agreement with numerical simulations (Zook *et al.* 1996). Recent Hubble Space Telescope (HST) observations constrained the grains to be smaller than 80 nm (Spencer *et al.* 1997). Hence, given the ejection speeds of more than 200 km s^{-1} , Io is a source for interplanetary and interstellar dust.

The jovian dust stream rates in the frequency-transformed *Galileo* dust measurements show different signatures, varying orbit to orbit. The varying frequencies from orbit to orbit are dependent on the spacecraft and dust detector geometry, on Jupiter's magnetosphere/plasma conditions, but also on Io itself, most likely its volcanoes' activity (see also Section 10.3.6).

10.3.4 Io's Dust Contribution

How significant is Io as a source of cosmic dust? How does the amount of dust ejected compare with other dust sources in the solar system? With a simple calculation, we can derive the total dust production rate of Io. Given the spread of Io dust along and away from Jupiter's equatorial plane, we assume a wedge-shaped emission pattern of dust originating at Jupiter, with a wedge opening angle of $\theta = 35^\circ$. Although *Galileo* measurements were obtained only along the jovian equatorial plane, this opening angle is justified by the *Ulysses* measurements. *Ulysses* measured the dust streams at 35° jovigraphic latitude after Jupiter flyby (cf. Figure 10.1). For a given impact rate R , particle density $\rho = 1.5 \text{ g cm}^{-3}$, particle radius $a = 10 \text{ nm}$, a detector sensitive area (averaged over one spacecraft spin revolution) of $A = 0.02 \text{ m}^2$ and a wedge radius $r = 30 R_J$ the total mass of dust ejected from Io per second is:

$$W = \frac{16}{3} \pi^2 a^3 \frac{R}{A} \rho r^2 \tan \theta \quad (10.2)$$

With $R \approx 0.1 \dots 100 \text{ min}^{-1}$ detected from 1996 to 2001 at $30 R_J$ the average dust ejection rate is $10^{-2} \dots 10 \text{ kg s}^{-1}$ (see also Figure 10.7). Summing under the Io and modulation product peaks of Figure 10.6 gives 60% of the total mass or 6×10^{-3} to 6 kg s^{-1} .

If we take a typical value of 1 kg s^{-1} of dust and compare it with 10^3 kg s^{-1} of plasma ejected from Io into the torus, the dust amounts to only 0.1% of the total mass released. These numbers indicate that Io is also a minor source for interplanetary dust compared with comets or main belt asteroids (Whipple 1987). Io, however, turns out to be a major dust source for the jovian system itself. The total mass of dust produced by Io as 10 nm-sized particles is comparable to the mass of dust ejected as micron-sized particles by

the other Galilean satellites, which have no volcanic activity (Section 10.5).

10.3.5 Monitoring Io's Volcanic Plumes

The jovian dust stream measurements can serve as a monitor of Io's volcanic plume activity. *Voyager*, *Galileo*, *Cassini* imaging observations have detected at least 17 volcanic centers with related plumes (Chapter 14). Most the plumes were sensed through the scattering of sunlight by dust particles entrained within the plumes. Ring-shaped surface deposits suggest that other plumes have been recently active as well. At least two major types of plume can be distinguished: large, faint plumes, with short-lived or intermittent activity (Pele-type) or small, bright, long-lived ones (Prometheus-type). Prometheus, the archetypal second category, is Io's most persistently active plume. Pele, one of the most powerful plumes on Io, has been observed at altitudes up to 460 km (Spencer *et al.* 1997, see also Chapter 14). The Pele plume is known to be rich in S_2 , as well as SO_2 (Spencer *et al.* (2000)). Although it has been suggested that the Pele plume may be a pure gas plume, plume observations can also be interpreted as being due to very fine ($\leq 80 \text{ nm}$) particulates according to Spencer *et al.* 1997.

It is of special interest to see whether variations in dust production rate deduced from the dust stream measurements can be related to the activity of individual plumes on Io or to the total thermal output of the satellite. The dust production rate of Io as derived from Eq. 10.2 is shown in Figure 10.7. A correlation of the dust emission with the activity of the most energetic plumes seems most promising. Only these plumes are expected to accelerate the grains to high altitudes so that they can collect sufficient charge from the ambient plasma to overcome the satellite gravity (Johnson *et al.* 1980, Ip 1996). A correlation of our in situ dust measurements with either *Galileo* or Earth-based plume imaging observations turned out to be very difficult. Because of the incomplete temporal coverage, only a very incomplete record of plume activity is available from direct sightings (McEwen *et al.* 1998, Keszhelyi *et al.* 2000). This is further complicated because plume activity sometimes changes on timescales of days to weeks.

A more complete history of Io's explosive eruptions has been derived from surface changes that they produce (Geissler *et al.* 2003). Changes in the surface appearance are most likely due to deposits by plume eruptions. Particularly large surface changes occurred at the north pole of Io, in the region South of Karei, Surt, Dazhbog, Thebes, and Tvashtar in the time periods indicated in Figure 10. Individual plume sightings are also indicated. The surface changes and plume sightings are in remarkable agreement with time periods when our in situ dust measurements showed high dust emissions. The extent of the observed changes implies that the eruptions which have caused them must have been among the most powerful during the *Galileo* mission.

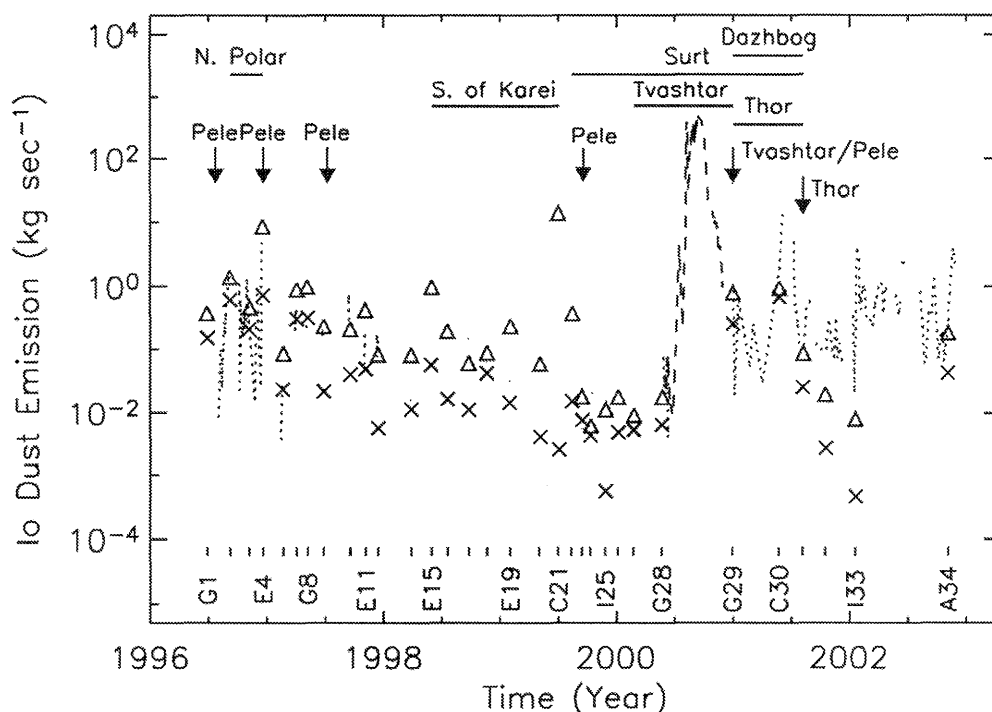


Figure 10.7. Dust emission rate of Io calculated with Eq. 10.2. Triangles and crosses denote the maxima and minima derived from measurements in the distance range $13 < r < 30 R_J$, respectively. The dashed line is for the G28 orbit in the range $30 < r < 280 R_J$, dotted lines show the remaining orbits with $30 < r < 400 R_J$. Thick horizontal bars indicate periods when large-area surface changes have occurred on Io (Geissler *et al.* 2003), arrows indicate individual plume sightings. Note that South of Karei probably erupted just before G1, and that Surt's eruption probably took place between G29 and C30. The data have been corrected for variation of the dust emission rate in the Io torus with jovian local time (Krüger *et al.* 2003d), and for a long-term change of the dust instrument sensitivity (Krüger *et al.* 2003b). *Galileo* peri-jove passages (vertical dashes) and orbit labels are indicated at the bottom. No dust stream measurements were detected during *Galileo* orbits 5 and 13 (Krüger *et al.* 2003a).

3.6 Long-Term Monitoring of Jovian Dust Streams

The *Galileo* mission offered the unique opportunity for long-term monitoring of the dust environment of Jupiter. Figure 10.8 shows the flux of jovian dust stream particles measured from 1996 (G1 orbit) to 2002 (I33 orbit) superimposed upon *Galileo*'s trajectory. In regions where no flux is shown, the dust streams were not detectable, because the dust detector was pointing in the wrong direction (most of the time when no flux is shown) or no dust data were transmitted to Earth. The *Galileo* dust instrument is affected by radiation-induced drop in sensitivity of about a factor of 20 between the early Jupiter mission in 1996 and the time of this writing (2003). Assuming the particle impact charge distribution as measured in 1996 (Krüger *et al.* 2001a, their figure 6) reflects the size distribution of dust stream particles when the instrument still had its nominal sensitivity, the resulting dust flux measured by the instrument is artificially too low late in the mission. The flux correction factor is one in 1996 and rises up to a value of 20 in 2002 (this correction factor applies to stream particles only because of the assumed impact charge distribution).

There are at least five interesting features in Figure 10.8:

First, fluxes of dust stream particles measured with *Galileo* are highly variable by about five orders of magnitude, between 3×10^{-3} and $6 \times 10^2 \text{ m}^{-2} \text{ s}^{-1}$. The cor-

responding number density of Io dust stream particles in the jovian environment varies from 10^{-8} to 10^{-3} m^{-3} (Table 10.1). Thus, the number densities of stream particles are usually much higher than the density in the faint jovian ring between the Galilean moons ($\sim 10^{-7} \text{ m}^{-3}$, Figure 10.20). Number densities in the dust streams are roughly comparable with those found in the dust clouds surrounding the Galilean moons (Figure 10.19), although the mass densities of dust in the clouds are an order of magnitude higher (Table 10.1).

Second, the dust flux is usually higher close to Jupiter, as one would expect if the dust source is located in the inner jovian system. The radial dependence of the dust flux measured with *Galileo* showed strong variations from orbit to orbit. Only in early 2001 (G29 orbit), was a nearly perfect r^{-2} drop of the dust flux measured, as one might expect from simple particle dispersion in space. Taking all orbits since 1996 together, slopes between -1 and -5 have been measured. These variations may be due to fluctuations in Io's dust production or the plasma conditions in the Io torus or both.

Third, in 2000 (G28 orbit), the dust flux measured by *Galileo* was about three orders of magnitude larger outside the magnetosphere ($\sim 10 \text{ m}^{-2} \text{ s}^{-1}$; radial distance from Jupiter about $280 R_J$) than within the magnetosphere (Krüger and Grün 2002). The reason for this "burst" is not yet understood. Interestingly, a strong Io period is evident in periodograms from this time interval whereas the 5- and

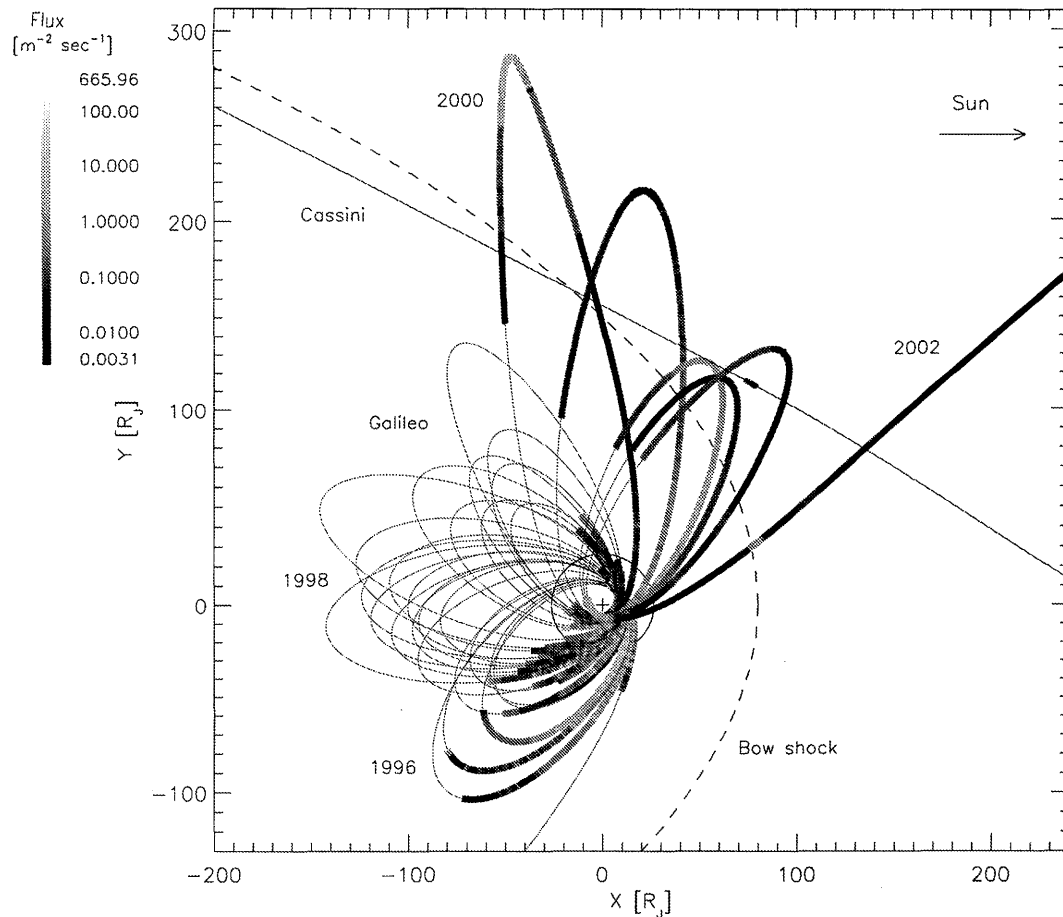


Figure 10.8. *Galileo*'s trajectory from 1996 to 2002 and *Cassini*'s trajectory at its Jupiter flyby in December 2000 and January 2001 projected on to Jupiter's equatorial plane. The fluxes of jovian dust stream particles measured with both spacecraft are superimposed on a gray scale (impact charges $Q_1 \leq 10^{-13}$ C). For calculating the impact direction of the particles, a typical trajectory of a 10 nm particle has been assumed (Grün *et al.* 1998). The *Galileo* flux has been corrected for aging of the instrument electronics. Because of strict operational constraints, *Cassini* measured the dust streams during a short period of 12 hr around Jupiter closest approach only. The rough location of the bow shock is indicated by a dashed parabola. The solid circle indicates Callisto's orbit and the Sun is to the right.

10-hr signature imposed by Jupiter is absent (Graps *et al.* 2001).

Fourth, such a high dust flux outside the magnetosphere did not always occur when *Galileo* was in this spatial region. A rather high flux ($\sim 1 \text{ m}^{-2} \text{ s}^{-1}$) occurred again in mid 2001 (C30 orbit), whereas other orbits showed a low dust flux at comparable spatial locations (G29, I31, I32, I33; $0.1 \dots 0.01 \text{ m}^{-2} \text{ s}^{-1}$).

Fifth, the data indicate a variation of the dust flux with jovian local time: significantly higher fluxes were measured on the dawn and the dusk sides than on the noon side of Jupiter (Krüger *et al.* 2003d). This is in good agreement with modeling results for the dust streams (Horányi *et al.* 1997); cf. Figures 10.12, 10.13) and is an additional proof that Io is the source of the dust stream particles. The dust data—together with detailed modeling of the particle charging and dynamics—may give important information about the plasma conditions in the Io torus (cf. Section 10.4.2).

10.3.7 *Cassini–Galileo* Joint Dust Stream Measurements

On 30 December 2000 the *Cassini* spacecraft flew by Jupiter providing a unique opportunity for a two-spacecraft time-flight measurement (*Cassini–Galileo*) of particles from a collimated stream from the jovian dust streams. Particles in a stream were detected with *Galileo* when the spacecraft was inside the jovian magnetosphere and close to the orbit of Europa (about $12 R_J$), and particles in the same stream were detected by *Cassini* outside the magnetosphere (at $140 R_J$). The *Cassini* data imply that particles of different sizes have different phases with respect to Jupiter's rotation (Kemmer *et al.*, in preparation), a result which is also seen in earlier *Galileo* data (cf. bottom line of Figure 10.3). The comparison of the measurements from both dust instruments, however, is hampered by the higher detection sensitivity of the *Cassini* detector with respect to the *Galileo* detector. Both instruments have detected stream particles with different sizes and, hence different phases. The analysis is ongoing and more detailed modeling to describe the phase relation of different-sized particles is in progress. The present analysis indicates particle speeds of about 400 km s^{-1} . This value

agreement with speeds for 5 nm particles as derived from analytical modeling (cf. Figure 10.16 and Section 10.4.4), earlier studies of the jovian dust stream dynamics (Zook *et al.* 1996).

1 JOVIAN DUST STREAM MODELING AND DYNAMICS

1.1 Modeling Approach

Motion of a charged dust stream particle in the jovian magnetosphere can be modeled by a transport code (Horányi *et al.* 1997) that follows the spatial and temporal evolution of a single dust particle or a dust density distribution in a magnetized plasma environment. The central body can be represented by a multipole expansion of its gravitational and magnetic fields. The density and the temperature of a many-component plasma environment can be defined as a function of coordinates and, if necessary, time. Given the gravitational and magnetic fields, and the plasma environment, the equations of motion can be integrated simultaneously with the equations describing the charging processes. The charging currents are dependent not only on the instantaneous plasma parameters but on the velocity, as well as the previous charging history of the dust grains.

1.2 Dynamics and Charging of Dust

We can approximate Jupiter's magnetic field by implementing the GSFC O₆ or VIP 4 model (Connerney 1993, Connerney *et al.* 1998), which is a multipole expansion of the planet's internal field. Jupiter's plasma is approximated using a plasma model, which is a fit to the *Voyager 1* and *Voyager 2* plasma measurements (Bagenal 1989, 1994). The model is defined in the centrifugal equator, which is the plane of symmetry for the plasma distribution in Jupiter's magnetosphere (Figure 10.9). The variation of the plasma density above and below the centrifugal equator is given by a simple height approximation. The model assumes a constant density ratio of 50% between singly ionized oxygen and sulfonium.

The density of the particles is in the range 1.35–1.5 g cm⁻³. These values give best agreement with charging and optical properties of insulating materials in general and with particle dynamics (Heck 1998, Graps 2001). The dust particles' optical properties are expressed via Q_{pr} , which is the radiation pressure coefficient. We implement Q_{pr} based on the particle's size and density (Burns *et al.* 1979).

Apart from Jupiter's point-mass gravity, the dust particles experience a variety of perturbing forces, both gravitational and non-gravitational. The range of the forces includes: solar radiation pressure, perturbations from Jupiter's oblateness, the Lorentz force that stems from the jovian magnetic field and electrostatic charges acquired by the grains in the jovian magnetosphere, and solar gravitational perturbations. Figure 10.10 gives the relative strengths of the forces as functions of the planetocentric distance r for grains with radii $a = 1 \mu\text{m}$ and $0.3 \mu\text{m}$. All of the forces depend strongly on the grains' size and/or planetocentric distance (Table 10.2). For this reason, populations of different-sized grains and those in different regions are dominated by

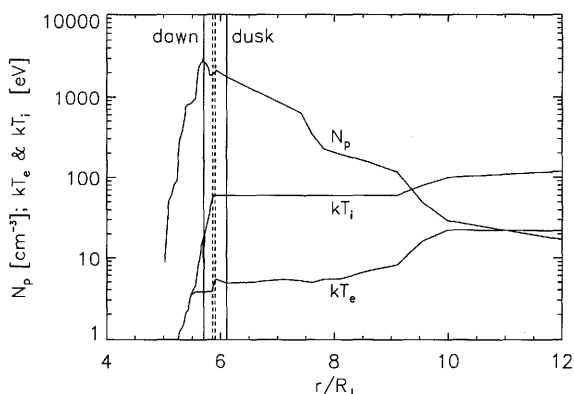


Figure 10.9. The plasma parameters in the centrifugal equator (density N_p , electron and ion temperatures: T_e and T_i) as function of distance from Jupiter. The range of Io's projection into the centrifugal plane (dotted lines) and the enlarged range due to the dawn-to-dusk offset of the entire plasma torus (continuous lines) are also marked.

Table 10.2. Properties of main forces acting on jovian grains.

Perturbing force	Size dependence ^a	Distance dependence ^b
Planetary gravity		
Jovian oblateness	$\propto a^0$	$\propto r^{-2}$
Solar gravity	$\propto a^0$	$\propto r^3$
Direct radiation pressure	$\propto a^{-1}$	$\propto r^2$
Electric force	$\propto a^{-2}$	$\propto r^0$
Magnetic force	$\propto a^{-2}$	$\propto r^{-3/2}$

^a Assuming that the radiation pressure efficiency factor and electrostatic surface potential do not depend on grain's radius.

^b Assuming an aligned corotating dipole magnetic field of Jupiter.

different subsets of the forces and accordingly, they exhibit quite dissimilar dynamics.

In any solar system plasma environment, the dynamics of small charged dust particles is strongly influenced, if not dominated, by the electromagnetic force acting simultaneously with gravity, drag and radiation pressure. Dust particles traversing various regimes adjust their electrostatic charges as dictated by the changing plasma conditions and they become "active electrostatic probes" continuously adjusting their surface potential towards the local equilibrium value. The equation of motion of a charged dust particle in a Jupiter-centered inertial frame is:

$$m \frac{d^2 \vec{r}}{dt^2} = \vec{F}_G + \vec{F}_{LP} + \vec{F}_L + \vec{F}_{SG} \quad (10.3)$$

where \vec{F}_G is Jupiter's gravitational force, \vec{F}_{LP} is the light pressure force, \vec{F}_L is the Lorentz force, and \vec{F}_{SG} is the solar gravitational force. For short lifetimes, neutral gas and plasma (Coulomb) drag forces on the dust particle can be neglected.

The gravitational acceleration due to Jupiter in an inertial joviocentric coordinate system in gaussian units is:

$$-GM_J \nabla \left(\frac{1}{r} + \frac{R_J^2}{r^3} J_2 P_2 \right) = \frac{\vec{F}_G}{m} \quad (10.4)$$

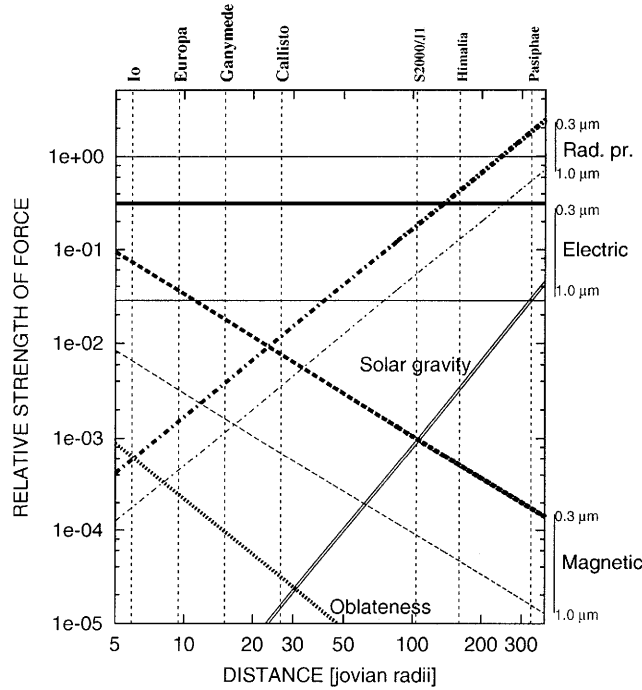


Figure 10.10. Strengths of the perturbing forces—radiation pressure, planetary oblateness, and the electric and magnetic components of the Lorentz force—acting on 0.3 (bold lines) and 1 μ m-sized (thin lines) spherical icy grains, as functions of their distance from Jupiter. Solid lines: electric force, dashed: magnetic force, dotted: oblateness, dash-dotted: radiation pressure, double solid: solar tidal gravity. Depicted are the ratios of the forces to the jovian point-mass gravity force. In calculation of the radiation pressure and Lorentz forces, compact spherical water ice grains with a unit radiation pressure efficiency and a constant surface potential of +5 volts (Horányi 1996, Burns *et al.* 1984, Burns *et al.* 1999) are assumed. Vertical dashed lines mark positions of the Galilean satellites, the innermost of the irregular moons S2000/J1, and of the largest moons in the prograde (Himalia) and retrograde (Pasiphae) irregular groups.

where r is the grain's joviocentric distance, with the constants: $G = 6.668 \times 10^{-8} \text{ g}^{-1} \text{ s}^{-2} \text{ cm}^3$, mass of the planet, $M_J = 1.9 \times 10^{30} \text{ g}$, its radius R_J and the perturbation from Jupiter's oblateness is described by the term with Legendre polynomial P_2 with coefficient $J_2 = 0.01474$.

The acceleration due to the light-pressure force is:

$$\frac{3J_0 Q_{\text{pr}}}{4\rho c d^2 a} \hat{r} = \frac{\vec{F}_{\text{LP}}}{m} \quad (10.5)$$

where \hat{r} is a unit vector pointing outward from the Sun, Q_{pr} is the radiation pressure coefficient, ρ is the dust particle's density, d is the planet's distance in AU from the Sun, c is the speed of light, a is the radius of a charged spherical particle, and J_0 is the solar energy flux at 1 AU ($1.36 \times 10^6 \text{ erg cm}^{-2} \text{ s}^{-1}$).

The Lorentz acceleration is given by:

$$\frac{Q}{m} \left(\vec{E}_c + \frac{\vec{v}}{c} \times \vec{B} \right) = \frac{\vec{F}_L}{m} \quad (10.6)$$

Here \vec{B} is the local magnetic field, and \vec{E}_c is the electric field, assuming a rigidly corotating magnetosphere (for up

to $50 R_J$): $\vec{E}_c = (\vec{r} \times \vec{\Omega}) \times (\vec{B}/c)$. If the dust particle located outside of the magnetosphere, then the electric field is driven by the convective motions of the solar wind.

The Lorentz force is by far the strongest force (100 times stronger than gravity) for nanometer-sized ejecta from and the strongest perturbation, comparable in magnitude with central gravity, for larger sub-micron particles ejected from Io and Europa. The Lorentz force naturally decouples into the "electric" part F_e , arising from the corotational electric field, and the "magnetic" part F_m (Eq. 10.6). If one assumes a dipole-aligned corotating magnetic field of the planet, which is an excellent approximation between the orbits of the Galilean satellites, it is easy to understand some of the salient features of the dynamics. The electric force effectively reduces Jupiter's mass: $M' = M(1 - L)$, where L is the ratio of the Lorentz force to the planetary gravity force for a grain, residing at rest in the jovian equatorial plane (Hamilton 1993):

$$L = \frac{Q B_0 R_J^3 \Omega}{G M_J c \rho a}, \quad (10.7)$$

where B_0 is the magnetic field strength at the planet's equator. This implies that a dust grain released from a comet moving in a nearly circular orbit, which charges up quickly, finds itself in an orbit with a non-zero eccentricity. Krüger *et al.* (2002a) presented an analogy with a dust grain released from a comet or asteroid which immediately feels an effective solar mass $M' = M(1 - \beta)$, where β is the ratio of radiation pressure to the solar gravity ratio (Burns *et al.* 1999). The magnetic force then causes the orbital ellipse to precess. Thus the sub-micron-sized ejecta from the inner Galilean satellites have orbits close to precessing ellipses. The smaller the grain size, the larger the typical eccentricities. If the grain radius is less than about $0.2 \mu\text{m}$, then the grains can be ejected from the circumjovian space into interplanetary space on escape orbits (Hamilton and Burns 1993; cf. Section 10.4.4). It is this mechanism that produces the jovian dust streams (Horányi *et al.* 1993b, Grün *et al.* 1998).

The gravitational acceleration due to the Sun is:

$$GM_S \left(\frac{(\vec{R} - \vec{r})}{|\vec{R} - \vec{r}|^3} - \frac{\vec{R}}{R^3} \right) = \frac{\vec{F}_{\text{SG}}}{m} \quad (10.8)$$

where M_S is the mass and \vec{R} the position vector of the Sun.

As grains traverse the various plasma regions their charge will not stay constant. A grain's charge can be followed via the current balance equation, summing over the currents: photoelectron emission I_ν , thermal ion and electron collection $I_{e,i}$, and secondary electron emission I_{sec} :

$$\frac{dQ}{dt} = \sum_k I_k = I_\nu + I_{e,i} + I_{\text{sec}} \quad (10.9)$$

Photoelectron emission current is generated when a photon of a UV photon releases photoelectrons and, hence, constitutes a positive charging current. Its magnitude depends on the material properties of the grain, i.e., its photoemission efficiency, and on the grain's surface potential which may, if positive, recapture a fraction of the photoelectrons. The ion and electron collection current is due to the flux of ions or electrons bombarding the particle from the ambient plasma.

Secondary electron emission current occurs when electrons or ions bombard grains with high enough energies to cause an ionization of the grain material and ejection of ions from the grain. The flux of secondary electrons depends on the grain's surface potential and on the energy of the plasma electrons/ions: E^P , which generally has a maximum value $\delta = \delta_M$ at an optimum energy $E^P = E_M^P$ (Mann 1981). The number of secondary electrons (yield) is the ratio of emitted to incident electrons. If $\delta > 1$, then positive dust charging occurs.

The parameter that sets the size range for the grains that can escape from the plasma torus is the secondary electron yield. In our earlier models (Horányi *et al.* 1993a,b), we used $\delta_M = 1$ and $E_M^P = 500$ eV. We found the characteristic average surface potential to be $\Phi \approx -30$ V in the cold plasma torus ($4 R_J \leq r \leq 6 R_J$) and $\Phi \approx +3$ V elsewhere. We found a good match between the simulations and the observations. However, the improved mass estimates from observations (Zook *et al.* 1996) can only be matched by adjusting the secondary electron yield parameters. For very small grains, δ_M is expected to increase (Chow *et al.* 1993). To allow for the escape of any dust grains in the size range $5 \leq a \leq 15$ nm we now choose $\delta_M = 3$. With this choice, the characteristic surface potential in the cold torus becomes approximately -5 V and $+6$ V elsewhere.

The dust particle's charge varies via these three currents, which are generated as the particle moves through the plasma. The charge equation (Eq. 10.9) is integrated simultaneously with the particle's acceleration (Eq. 10.3). For very small nanometer-sized grains, Eq. 10.9 must be solved with some care to recognize the quantized nature of electrostatic charges.

The charge of an escaping dust particle is a function of its position in both magnetic and inertial coordinates, reflecting the plasma density and temperature variations in space and time along Io's orbit. The displacement of the plasma torus, due to a cross-tail electric field, results in a strong dawn-to-dusk asymmetry in the plasma conditions that influences the escape of the dust particles. In general, charges of the grains are more negative on the dawn side of the torus where the electron temperature is lower, hence secondary electron production is reduced (Figure 10.11).

Dust equilibrium potential is reached when the sum of all of the charging currents is zero. The dominant electron capture from the plasma leads to negative charges, and other charging processes—ion capture, secondary electron emission and photoelectron emission—facilitate positive currents. Secondary electron and photoelectron emission charging processes are highly material dependent. The time to acquire the equilibrium charge may be longer than the flight trajectory time of the particle, therefore it is worthwhile to investigate equilibrium charging times.

Numerical charging experiments (Graps 2001) show that the dust particles rarely reach an equilibrium potential as they travel through the jovian magnetosphere. The dust particles in the size range 5–25 nm within Jupiter's magnetosphere needed approximately 1–5 hr to reach equilibrium potential (the smaller particles needed longer times). Beyond $50 R_J$, the particles do not reach equilibrium charge potential in the numerical experiment representing a ten-hour charging time. In the plasma conditions of the solar wind, the particles never reached equilibrium in the ten-

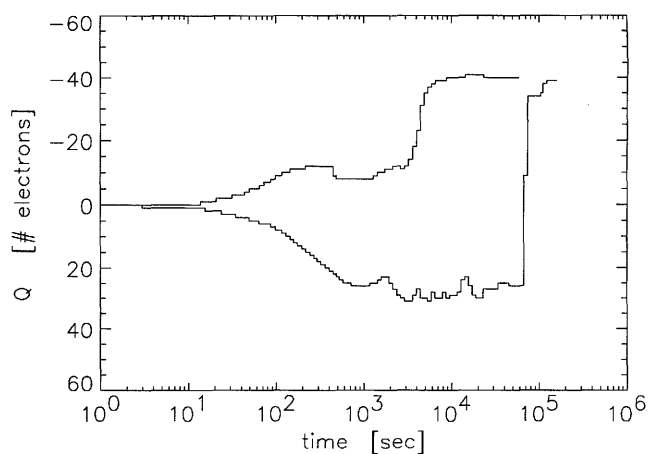


Figure 10.11. The charge history of 2 dust grains that were started from Io at longitudes $\lambda = 90^\circ$ (dusk) and 270° (dawn). The grain starting on the dawn side collects electrons (charges negatively) and remains confined for approximately a day. The grain starting on the dusk side of the torus is losing electrons (charges positively) and escapes from the Io plasma torus in less than an hour (Horányi *et al.* 1997).

hour time span of the numerical experiment. Using a set of particle material properties and secondary electron and photoemission parameters for a 10 nm radius sulfur particle, the particle has a surface potential of about $+6$ V everywhere, except for the region inside of $8 R_J$, where the potential is lower.

10.4.3 Jovian Dust Stream Dynamics

The suggested mechanism to eject dust particles from within the jovian magnetosphere matched the size and velocity range of the observed stream particles by recognizing that these grains become positively charged and can gain energy from the corotational electric field (Horányi *et al.* 1993a). Dust grains escaping Io enter the cold plasma torus where they become negatively charged and remain confined there. Grains that visit the outer hot regions of the plasma torus change their sign of charge to positive, due to secondary electron production. Once a grain charges positively, it will be accelerated by the outward pointing corotational electric field. The periodic nature of the observed dust streams on *Ulysses*' approach (Figure 10.1) to Jupiter is most likely caused by the changes in the azimuthal component of the solar wind magnetic field, that periodically accelerates these particles towards and away from the ecliptic plane (Hamilton and Burns 1993). Our current best estimate for the size range of the dust grains seen by *Ulysses* and *Galileo* is $5 \leq a \leq 15$ nm and their velocity $v \geq 200$ km s⁻¹. The terminal speed of the particles can be approximated by (particle radius a_{nm} in nanometers):

$$v_t \approx 3000/a_{nm} \quad (\text{km s}^{-1}) \quad (10.10)$$

This simple speed versus size relationship assumes a centered aligned dipole magnetic field, but it holds up remarkably well in our detailed computer simulations (cf. Figure 10.16).

Using the particles and fields model of the jovian magnetosphere (Section 10.4.2), Figure 10.12 shows a sample of

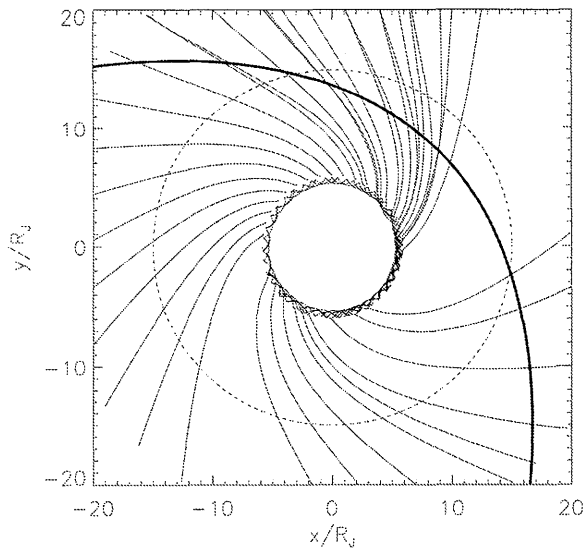


Figure 10.12. The trajectories of 10-nm radius dust particles projected on to Jupiter's equatorial plane. Thirty-six grains were started uncharged, uniformly spaced along Io's orbit with Keplerian initial velocities. The trajectories of the *Galileo* spacecraft (G2 orbit in 1996, thick line) and the moon Ganymede (dotted line) are also marked (Horányi *et al.* 1997).

dust particle trajectories escaping from the torus. We placed 36 grains ($a = 10$ nm) uniformly along Io's orbit and followed their trajectories and charges simultaneously. The pattern of the trajectories would change by changing the initial phase of the magnetic field. The grains do not stay confined to the equatorial plane due to the "tilted" nature of Jupiter's magnetic field. Grains starting on the dusk side swiftly escape from the Io plasma torus, but grains on the dawn side remain captured for longer periods of time.

Figure 10.12 predicts a strong asymmetry of the ejected dust fluxes with jovian local time: higher fluxes are expected on the dawn and dusk sides of Jupiter than at noon. The theoretical expectation from our modeling is shown in the top panel of Figure 10.13. This is remarkably confirmed by six years of *Galileo* dust measurements at Jupiter. It shows that the plasma model, the description of the charging processes and the dynamics of the grains used in the model reproduce the long-term behavior of the observations. In particular, the plasma conditions in the torus are well represented as they are crucial for dust charging there. Models without the torus' dawn-dusk asymmetry do not show any local time dependence of the dust flux. Thus, dust stream particles can be used as tracers of the plasma conditions in the Io torus.

Though the exact trajectory of a grain is a function of its initial position and size, the general nature of the trajectories, as projected on to the equatorial plane of Jupiter, remains as shown for all grains in the size range of $5 \leq a \leq 15$ nm. This general shape is likely to be responsible for the sudden 180° shift in the observed dust impact directions within a day around perijove passage of *Galileo* (Figure 10.5, see also Grün *et al.* 1997, 1998, Heck 1998; note that the shift occurred several hours earlier than expected for radial particle trajectories).

In these initial simulations, we assumed a constant pro-

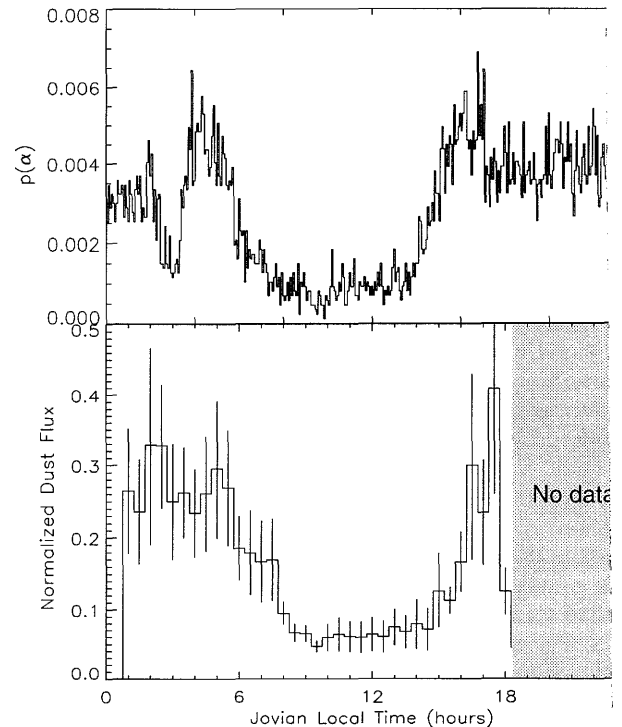


Figure 10.13. Flux of jovian dust streams as a function of jovian local time. Top: distribution of dust particles crossing Ganymede's orbit within $\pm 3^\circ$ jovigraphic latitude derived from dynamical modeling (Horányi *et al.* 1997). Bottom: Dust stream measurements from 33 *Galileo* orbits. Flux measurements for each orbit have been normalized to the interval [0,1] and then added in each local time bin. Measured fluxes have been multiplied by $(r/6R_J)^2$ to eliminate the distance dependence of flux due to the motion of *Galileo* about Jupiter (Krüger *et al.* 2003d).

duction rate of dust from Io. Figure 10.14 shows snapshots from these simulations. The enclosed CD contains computer animations showing the complex time-dependent structure of the "dusty ballerina skirt" comprised of tiny grains ejected from the magnetosphere of Jupiter. We captured the general features of the observations as far as the temporal and minute variabilities are concerned, demonstrating that the basic physical ideas of charging and dynamics in this model are correct. However, many of the observed features are not yet explained in these simulations.

10.4.4 Sizes of Dust Ejected from the Jovian Magnetosphere

A window of particle sizes exists for which dust particles can escape from traveling in Keplerian orbits in Jupiter's magnetosphere. This particle size is strongly dependent on the charging assumptions, especially the secondary electron emission material assumption.

For $L \ll 1$, the Lorentz force is a perturbation to the gravitational force, therefore dust particles follow Keplerian orbits. For $L \gg 1$, the gravitational force is a perturbation to the Lorentz force, therefore, the dust particles act like plasma ion and electron particles, which gyrate about the planet's magnetic field lines. Between these two regimes lie

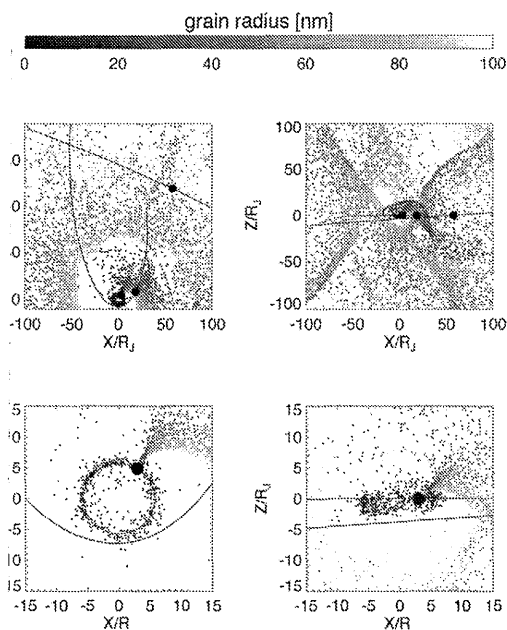


Figure 10.14. A snapshot of the positions of the dust grains ejected from Io. The surface potential of the grains was kept constant ($\phi = 5$ V). The top panels show the spatial distribution on large scales, while the bottom panels only show the immediate vicinity of Io (the left panels show the positions projected on the equatorial plane and the right panels show the positions projected on to a meridional plane). The “color” code represents the particle radius in the range of 5–100 nm (blue–red). The thick continuous lines show the trajectories of *Galileo* and *Cassini* during closest approach of the later one to Jupiter (the dots on the trajectories mark the positions of the spacecraft at the time of *Galileo*’s closest approach). This snapshot is from a computer simulation that is recorded on the accompanying CD.

find a window $a_*^{\min} < a_* < a_*^{\max}$ of particle sizes a_* for which positively charged dust particles can escape from the jovian magnetosphere. The particles with the smallest grain sizes in this window a_*^{\min} experience a weaker Lorentz force and fewer gyroradii than those even smaller particles which are inescapably bound to the magnetic field lines, and the particles with the largest grain sizes in this window a_*^{\max} barely have enough energy to escape from being bound gravitationally to Jupiter (Hamilton and Burns 1993, Horányi 1996, Krivov *et al.* 2001).

To find the *smallest* grain size for grain ejection, we start with the gyration of a tiny grain along Jupiter’s magnetic field lines (Horányi 1996, Graps 2001), assume a magnetic field for an aligned centered magnetic dipole, and describe the motion of a grain bound to the magnetic field line in a guiding centered approximation (Morfill *et al.* 1980). The grain radius, a , using these assumptions, is:

$$a_{\min} \approx \left[\frac{0.1\varphi B_0 R_J^3}{300\omega\rho 4\pi c r^2} \right]^{\frac{1}{2}} \quad (10.11)$$

Using this equation, the smallest grain size for ejection is approximately 8 nm, changing to a particle radius several nanometers larger (smaller) if the secondary electron yield of the electron/ion impact energy is larger (smaller).

To find the *largest* grain size for ejection from Jupiter’s magnetosphere, we begin with Hamilton and Burns (1993),

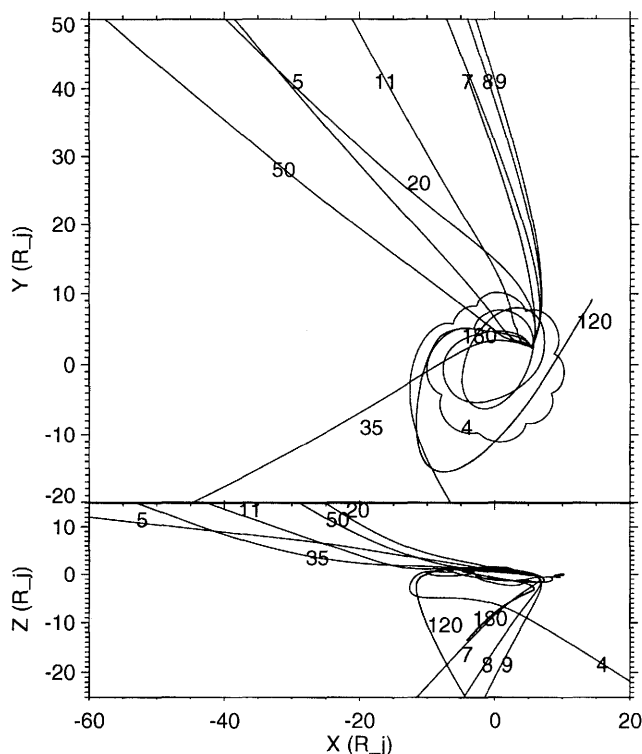


Figure 10.15. Trajectories for jovian dust stream particles of different radii labeled in nm, which were released traveling at a circular Keplerian velocity just outside of the Io plasma torus at 6.2 R_J . The material properties are defined in Section 10.4.2.

and solve for a :

$$a_*^{\max} \approx \sqrt{\frac{0.0057\varphi}{\rho L}} \quad (10.12)$$

This last expression gives a convenient relationship for the grain size as a function of potential, density and ratio L , where the unit of φ is volts, and the unit of density is g cm^{-3} . If $L \geq (1/2)$, the grain will be ejected from the circumjovian space into interplanetary space in a parabolic or hyperbolic orbit (Hamilton and Burns 1993, Krivov *et al.* 2002a). Therefore, the above expression gives the largest grain size for ejection. Using this equation, the largest grain radius for ejection is approximately 200 nm.

Figure 10.15 illustrates simulated trajectories of density $\rho = 1.5 \text{ g cm}^{-3}$ spherical particles, with their radii labeled in nanometers, which were released at a circular Keplerian velocity just outside the Io plasma torus at 6.2 R_J . The particle dynamics are simulated by the particles and fields model described in Section 10.4.2. The initial surface charge potential of these particles was +3 V, and secondary electron emission current of the dust particles is based upon material property parameters of $\delta_m = 3.0$, $E_m = 300 \text{ eV}$. For these parameters, a particle of size 4 nm is bound, and size 5 nm is ejected. If one increases the particle size, the particles continue to be ejected from this location, until their radius is at about 100 nm, when gravity dominates the particle’s movement. These simulated trajectories indicate different particle sizes for ejection than the theoretical values (Eq. 10.11, Eq. 10.12), because the theoretical values use simplified assumptions for Jupiter’s magnetic field.

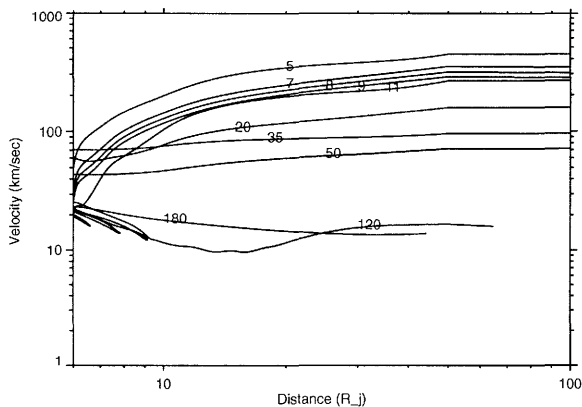


Figure 10.16. Velocities vs. distance from Jupiter for jovian dust stream particles of different radii, labeled in nanometers, starting from +3 V, and using the material properties as defined in Section 10.4.2.

The corresponding velocities can be quite high for the smaller ejected dust stream particles. A 5 nm particle is traveling at a speed roughly 200 km s^{-1} at $12 R_J$, and will reach about 400 km s^{-1} outside of the jovian magnetosphere at $130 R_J$. In Figure 10.16, we show simulated velocities of different sizes of dust stream particles using the same set of particle parameters which resulted in the trajectories of Figure 10.15.

10.5 DUST CLOUDS SURROUNDING THE GALILEAN SATELLITES

10.5.1 Measurements

During its orbital tour about Jupiter, the *Galileo* spacecraft had a total of 32 targeted flybys of all four Galilean satellites. During many of these encounters between 1995 and early 1999, the impact rate of dust grains showed a sharp peak within about half an hour centered on closest approach to the satellite (Figure 10.5, Grün *et al.* 1996b, 1997, 1998, Krüger *et al.* 1999a). These peaks indicated the existence of dust concentrations in the close vicinities of all four Galilean moons. During the flybys at the Galilean satellites after mid 1999, the spacecraft orientation prevented the detection of dust particles close to the moons.

The geometry for *Galileo* dust detections during a typical satellite flyby is depicted in Figure 10.17. Because the *Galileo* detector scans about half a hemisphere during one spacecraft revolution, the spacecraft orientation during each dust impact (rotation angle) can be used to identify dust impacts around the Galilean moons; here, particle impacts at rotation angles $180^\circ \leq ROT < 360^\circ$ are compatible with dust impacts from the ram direction. Impacts from this direction occur only in the vicinity of the moon, and they are concentrated towards satellite closest approach. Impacts from the opposite direction, $0^\circ \leq ROT < 180^\circ$, do not show such a concentration (Krüger *et al.* 1999e, 2000, 2003e). The latter are mostly due to jovian dust stream particles which have been detected throughout the jovian magnetosphere (Section 10.3). Hence, the impact direction of particles with $180^\circ \leq ROT < 360^\circ$ measured at Ganymede and Europa points to an origin of the particles from the satellite itself.

For Callisto and Io, the impact direction could not be used as an independent parameter for particle identification because the jovian dust stream particles approached the moons from the same direction as potential satellite particles in case of Callisto, and from almost all rotation angles in case of Io.

The mean impact speeds for particles in this range and impact direction are within the measurement uncertainty in very good agreement with the spacecraft speed relative to Ganymede and Europa (8 km s^{-1} and 6 km s^{-1} , respectively). Only very few cloud particles have been detected at Io, and their mean impact speed is also in agreement with the spacecraft speed relative to this moon. In case of Callisto, the particle speeds could not be independently checked. Particles with impact speeds below 10 km s^{-1} show a slight concentration towards the surface of Callisto. This result—together with the impact direction—indicates that the detected particles belong to steady-state dust clouds surrounding the moons. The concentrations of dust towards the moons leave no doubt that the moons themselves are the sources, because their gravitational and electromagnetic forces are too weak to appreciably focus interplanetary or interstellar dust. As there are no indications of volcanic activity on these three Galilean moons, the most likely source is the continuous ejection of debris via bombardment of the satellites' surfaces by interplanetary micrometeoroids. The cloud particles detected at all four Galilean moons have sizes between one and two orders of magnitude larger than the stream particles (cf. Table 10.1). In the case of Io, this may be a particle origin from its volcanic plumes unlikely. It should be noted that, contrary to the dust stream particles, the cloud particles are well within the calibrated range of the dust instrument, so that the measured impact speeds are reliable within the measurement uncertainty.

The particle mass distributions, obtained by applying the calibration of the dust instrument, are in agreement with power laws with slopes between 0.5 and 1 down to particle masses of 10^{-16} kg (which is the detection threshold of the dust instrument). Assuming a particle density of 1 g cm^{-3} , the majority of the detected grains is in the size range $0.5 \mu\text{m} \leq a \leq 1.0 \mu\text{m}$ (Krüger *et al.* 2000, 2003e) in agreement with theoretical expectations.

The number density of the particles in the dust clouds surrounding all four moons is shown in Figure 10.18. It is up to three orders of magnitude larger than the dust number densities measured with *Galileo* in the region between the Galilean satellites (Thiessenhusen *et al.* 2000; see also Figure 10.20). The number densities measured for the four moons are in remarkable agreement. This indicates that the properties of the dust clouds are very similar for all of the moons. The power law fit to the data with slope -2.2 ± 0.36 is close to the expected value of -2.5 (Krivov *et al.* 2003).

The optical thickness of the clouds is too low to be detectable with imaging techniques. Only a highly sensitive detector of the *Galileo/Ulysses* type could recognize a sufficient number of grains to detect these clouds. For example, only 64 cloud particles impacted the detector during eight flybys at Europa.

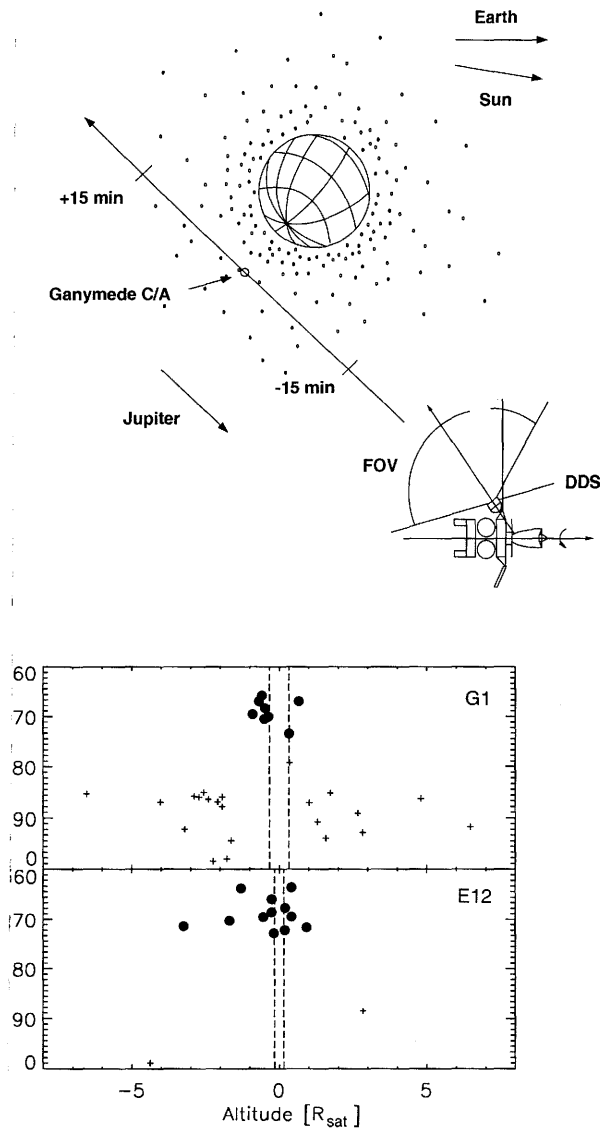


Figure 10.17. Top: *Galileo*'s trajectory and geometry of dust detection during a typical satellite flyby. The spacecraft is shown in nominal orientation with its antenna pointing towards Earth and the dust detector facing the anti-Earth hemisphere. The dust detector is shown in an orientation where particles belonging to a cloud of dust surrounding the satellite can be detected ($\theta_T = 270^\circ$). Bottom: Sensor direction (rotation angle, ROT) versus altitude of *Galileo* above the surface of the satellite at the time of dust impact for two typical satellite flybys (G1 Ganymede flyby and E12 Europa flyby). The altitude range shown corresponds to a time interval of ≈ 1.6 hr. The direction to the satellite is about 270° during approach. Vertical dashed lines indicate distance of closest approach to the satellite. Here we plot only flybys for which we have a complete set of parameters (Krüger *et al.* 2000). The apparent concentration of particles within $5 R_{\text{sat}}$ is due to an increased data transmission rate near Ganymede. Satellite radius $R_{\text{sat}} = 1560$ and 4 km for Europa and Ganymede, respectively.

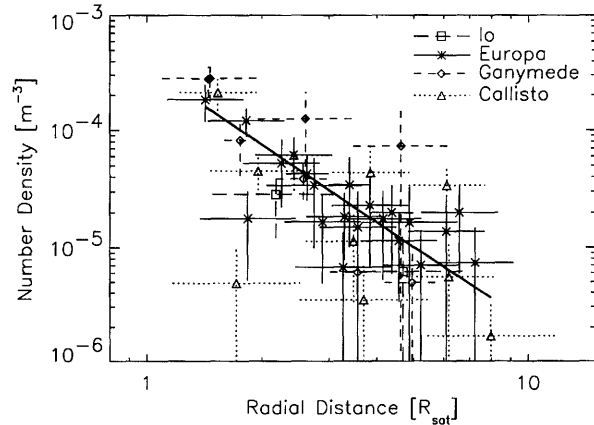


Figure 10.18. Number density of dust as a function of radial distance from the center of Io (data from 1 flyby), Europa (8 flybys), Ganymede (4 flybys) and Callisto (3 flybys). The radial distance is shown in units of the satellite radius $R_{\text{sat}} = 1818, 1560, 2634, 2409$ km in the case of Io, Europa, Ganymede and Callisto, respectively. Vertical error bars reflect statistical uncertainty due to the small number of impacts. The solid line is a least squares fit to the measured number densities for all moons (Krüger *et al.* 2003e).

10.5.2 Dynamics of Grains in Circumsatellite Dust Clouds

A model of a circumsatellite dust cloud is constructed in two steps (Krüger *et al.* 2000, Krivov *et al.* 2003). First, one considers the production rate of dust from the surface of a parent satellite. This requires a chain of estimates: the mass flux and typical speed of projectiles are estimated from existing models of the interplanetary meteoroid environment, corrections are made for gravitational focusing by Jupiter, mass production rate is estimated using impact experiment data on the ejecta yield, etc. This results in N^+ , the number of dust grains (above a given mass or size), ejected from the surface per second.

Given the ejecta production rate, the second step is to model the steady-state distribution of dust around the satellite. This step requires a number of assumptions and extensive analytic work. The initial speed distribution of ejecta is postulated as a power law (see, e.g., Stöffler *et al.* 1975, Hartmann 1985)

$$\Psi(>u) = (u/u_0)^{-\gamma} \quad (u \geq u_0) \quad (10.13)$$

where $\Psi(>u)$ is the fraction of the material ejected at speeds $>u$. In Eq. 10.13, u_0 and γ are constants that depend on the target material and mass, as well as speed and mass of the projectiles. Typically, the lower cut-off values u_0 of the ejecta speed are tens of m s^{-1} . The distribution slope γ ranges from about 1 for loose, regolith-like targets to about 2 for harder surfaces such as low-temperature ice. Next, we assume that all the material is ejected into a cone normal to a target surface, the semi-opening angle varying between 0° (normal ejection) and 90° (isotropic ejection). Two populations of the debris particles are considered: those which move on ballistic trajectories and therefore fall back to the satellite shortly after they are ejected, and those which are fast enough to escape from the moon into circumjovian space. We assume that these ejecta move on Keplerian tra-

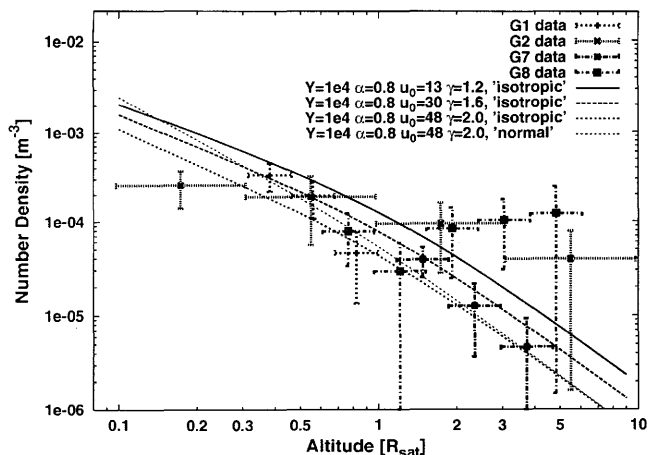


Figure 10.19. Number density of dust in the dust cloud around Ganymede. Lines: number density predicted by the model in the cases of isotropic and normal ejections for several choices of model parameters—yield Y , cumulative mass distribution of ejecta α , lowest ejecta speed u_0 (in m s^{-1}), and the slope of the ejecta speed distribution γ . Symbols with error bars: number density derived from the *Galileo* measurements during its G1, G2, G7, and G8 flybys.

jectories—pieces of ellipses and hyperbolas, respectively. This is a good approximation for all Galilean satellites, especially for micron-sized dust which is not vulnerable to non-gravitational forces. It is also assumed that the circumsatellite dust cloud is in a steady state. Finally, we neglect possible effects of non-isotropy of the impactor flux (e.g., Colwell 1993) and assume that the cloud is spherically symmetric. Thus, possible variations in the spatial density, which may be caused by spatial or temporal variations of a dust cloud, are not covered by the present model.

Under this set of assumptions, exact solutions for the number densities of dust both in ballistic and unbound orbits can be derived (Krivov *et al.* 2003). An approximate expression for the number density of dust grains ejected into elliptical orbits, which dominate a cloud at distances of several satellite radii, is

$$n_{\text{bound}}(x) = \frac{N^+}{2\pi R_{\text{sat}}^2 u_{\text{esc}}} \frac{\gamma}{u_{\text{esc}}} \left(\frac{u_0}{u_{\text{esc}}}\right)^\gamma x^{-5/2} K(x) \quad (10.14)$$

where $x \equiv r/R_{\text{sat}}$ is the distance measured in satellite radii, u_{esc} is the escape speed from the surface, and the last factor is close to unity: $K(x) = 1 + O(1/x)$. Interestingly, the angular distribution of ejecta velocities affects the result only weakly: the above expression holds true both in normal and isotropic ejecta cases, and only the correction term $O(1/x)$ in $K(x)$ differs. Equation 10.14 shows that the number density decreases with increasing distance from the satellite center approximately as $r^{-5/2}$. That the slope is steeper than 2, reflects the fact that larger distances can be reached only by particles ejected at higher speeds, which are less abundant than slower ejecta.

To illustrate how the model works, and how the modeling results compare to the *Galileo* data, we choose Ganymede, the largest of the Galilean moons. Figure 10.19 shows the number density of the dust cloud around Ganymede for several choices of the model parameters and for both normal and uniform ejection. The number density

derived from the *Galileo* dust data, obtained during its flybys of Ganymede, is plotted in the same figure. Figure 10.19 shows a satisfactory agreement between the model and the measurement results. The agreement is good for G1 and G7 flybys and worse for G2 and G8 flyby data. The latter are less reliable, however, because in these cases correction factors for incomplete data transmission were introduced in data processing. For G1 and G7 flybys, the radial slope of the number density was found to be 2.3—close to what Eq. (10.14) predicts. For a detailed comparison between the model and *Galileo* data, the reader is referred to Krüger *et al.* (2000). We note that any tangible improvement of the poorly known parameters (yield, slope of ejecta speed distribution, etc.) is unfortunately not possible, because of the scarcity of the data, especially at small and large altitudes. We can only state that the parameters chosen are compatible with the data.

One goal is to check the data for signatures of a leading trailing asymmetry of the ejecta clouds, which can be expected from the orbital motion of a satellite with respect to the field of impactors. We can define the asymmetry factor as the ratio of the dust production rate at the apex point on the satellite surface to the production rate averaged over the surface. The factor depends on the satellite, varies with time, and may in some cases be close to one (nearly all dust is ejected from the leading hemisphere). However, the resulting asymmetry of the dust density in the cloud rapidly smears out with increasing distance from the moon, decreasing to about a half its surface value at $3R_{\text{sat}}$ and about one tenth at $10R_{\text{sat}}$ (Šremčević *et al.* 2003). Thus the asymmetries in the clouds may not be as pronounced as they seem.

As follows from elementary estimates, the particles that reach an altitude of one satellite radius must have a minimum velocity in excess of 2 km s^{-1} . This confirms laboratory results that some of the hypervelocity impact ejecta from icy targets attain very high speeds (Frisch 1992). Nevertheless, more than a half of the grains which could be found (and have been actually detected by *Galileo*) at altitudes less than about eight satellite radii above the surface, are not the particles escaping into jovian space. They are slower ejecta, destined to fall back to Ganymede typically within several minutes to several hours after ejection. Such grains surround the satellite all the time as a result of continuous bombardment of the surface by interplanetary dust particles (IDPs). Further out, starting from distances of $\approx 8R_{\text{sat}}$ (Ganymede radius $1 R_G = 2634 \text{ km}$), the escaping grains start to dominate the number density.

It seems useful to give some general estimates concerning the mass budget of the dust cloud of Ganymede. The mass flux of IDPs bombarding the satellite surface is estimated to be $\sim 3 \times 10^{-2} \text{ kg s}^{-1}$ (dominated by IDPs with $m \sim 10^{-8} \text{ kg}$). With the characteristic yields of $\sim 10^4$, we then estimate that as much as $\sim 10^2$ to 10^3 kg s^{-1} of the moon's surface material is ejected into space. Depending on the ejecta speed distribution adopted, the mean lifetime of the ejecta ranges from tens of seconds to several hundred seconds. Note that these values are dominated by the slowest ejecta—for the grains that reach the altitudes of several satellite radii the flight times are several hours. We, therefore, derive an estimate of the total amount of dust contained in a steady-state cloud around Ganymede: 10^3 to 10^5 kg .

ion of about 10^{-4} to 10^{-3} of the ejecta escape from satellite. It gives the injection rate of the material into jovian space of $\sim 10^{-2}$ to 10^0 kg s $^{-1}$, which may be variable with the influx rate of IDPs to the Ganymede ce. The ejected material goes into orbit around Jupiter. Gas escaping from the Galilean satellites are probably responsible for some of the impact events detected by the dust instrument in the inner jovian system (Section 10.6).

A FAINT DUSTY RING BEYOND JUPITER'S GOSSAMER RINGS

1.1 Measurements

From Io dust streams (Section 10.3) and circumsatellite ejecta-clouds (Section 10.5) the in situ *Galileo* measurements have so far revealed at least one more population of jovian dust: since the beginning of *Galileo's* orbital tour of Jupiter the dust detector has measured more than 100 impacts of mostly micron-sized grains widely distributed throughout jovian space. Although most of the impacts occurred in the region between Europa's and Callisto's orbit (10 to 26 R_J from Jupiter; (Grün *et al.* 1998, Krüger *et al.* 1999)) impacts were also detected out to 100 R_J and beyond (Krivov *et al.* 2002b). These grains form a tenuous dust ring around Jupiter with a number density of 500 km $^{-3}$ at Europa's orbit (Thiessenhusen *et al.* 2000, Krivov *et al.* 2002a; see Section 10.20). The spatial locations where these grains were detected, the impact directions and the charge signals imply that there are actually two populations: besides a population of grains on prograde orbits about Jupiter, another population on retrograde orbits must exist as well (Colwell *et al.* 1999b,a, Thiessenhusen *et al.* 2000). The ring of material formed by these grains escaping from the Galilean moons is so tenuous for optical detection.

Indications for the existence of the ring can already be found in earlier measurements by *Pioneer 10/11* and *Voyager*: 12 meteoroid penetrations have been recorded with *Voyager* within 45 R_J from Jupiter (Humes *et al.* 1974) and *Voyager* has recorded 9 impacts of micron-sized dust grains in the same spatial region. Two-thirds of the *Ulysses* impacts were recorded within a jovigraphic latitude of about 35° after their flyby.

Further, Krivov *et al.* (2002b) analysed the *Galileo* dust measurements of the outskirts of the jovian system, outside the gossamer rings. The spatial distribution of impacts, calibrated masses and speeds of grains, and impact directions, of 99 individual impact events are fully compatible with planetary grains orbiting Jupiter in the outermost part of the jovian system. These grains have moderate eccentricities and a wide range of inclinations—from prograde to retrograde orbits. The radial number density profile of the micron-sized dust derived from the data is nearly flat between about 50 and 300 R_J. The absolute number density level (~ 10 km $^{-3}$), being almost two orders of magnitude lower than the density in the “Galilean dust ring” near Europa's orbit, surpasses by a factor of ten that of the interplanetary background. The mass distribution of the detected grains shows a gap around 10^{-14} kg (radius of $1 \mu\text{m}$). The grains with masses larger than this are most probably planetary particles, and their sources are identified with the outer irregular satellites of Jupiter (see Section 10.6.2).

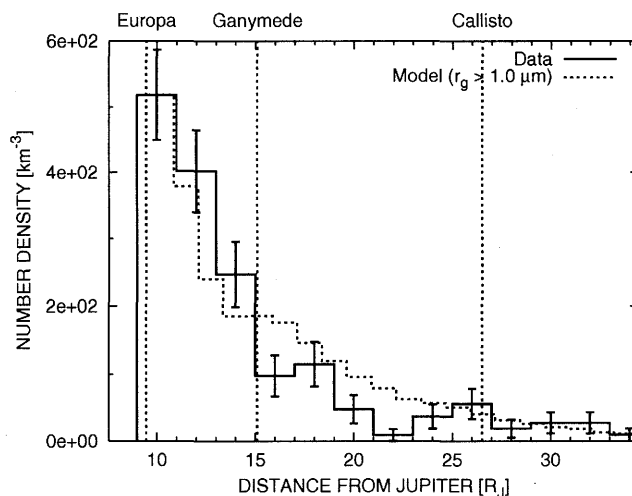


Figure 10.20. Number density of dust in the “Galilean” ring. Solid line with error bars: *Galileo* measurements. Dashed line: modeling results. Note that the modeled profile was scaled to the same peak value as the measured profile has. The scaling factor applied is 0.52. Vertical dashed lines mark positions of the Galilean satellites.

The distribution of dust between Europa's and Io's orbits is not very well explored yet. *Galileo* has traversed this region several times since October 1999. These data indicate an increase in the number density between Europa and Io.

Looking further inward towards Jupiter, between Io's orbit at 5.9 R_J and the outer extension of the gossamer ring at about 3.1 R_J, extremely little is presently known about the dust environment. Although *Galileo* has traversed part of this region during orbit insertion in December 1995, dust measurements are very patchy because the instrument had to be saved from the hazards of Jupiter's radiation environment. However, a few micron-sized dust impacts were detected inside Io's orbit (Grün *et al.* 1996b, Krüger *et al.* 1999b; see also Section 10.7).

10.6.2 Sources and Dynamics of Larger Grains in Orbits about Jupiter

To explain “big” impact events registered by the *Galileo* dust detector in the region of the Galilean satellites and beyond, we shall now discuss probable sources of dust, and the grain dynamics. Although a minor fraction of these impacts can be attributed to the background particles, mostly interplanetary and interstellar ones, these external populations alone fail to explain the measurements. Therefore, internal sources of dust inside the jovian system are required. Three major mechanisms have been suggested:

- (i) *Magnetospherically captured interplanetary grains.* The jovian magnetosphere can efficiently trap interplanetary and interstellar particles in bound orbits about Jupiter (Colwell and Horányi 1996, Colwell *et al.* 1998b,a). The capture is especially efficient for particles about $1.0 \mu\text{m}$ in radius. The resulting orbits have been shown to be mostly retrograde and to mostly lie well inside the orbit of Callisto.
- (ii) *Dust from the Shoemaker-Levy 9 comet.* The frag-

mentation of the Shoemaker-Levy 9 comet that took place about a year before the comet crashed into Jupiter is believed to have injected copious amounts of dust material into the jovian system (Horányi 1994). As in the previous case, most of the debris would fall into retrograde orbits and spread predominantly to the inner jovian system, inside the Europa orbit.

(iii) *Impact production of dust from satellite surfaces.* This standard mechanism implies that hypervelocity impacts of external projectiles (e.g., interplanetary micrometeoroids) eject material from the surfaces of the jovian satellites. This is the same mechanism that produces the dust clouds around the Galilean satellites described in Section 10.5—the only difference is that we now focus our attention on the ejecta that are fast enough to escape from the parent bodies. Thus, the Galilean satellites could be sources for prograde dust detected by *Galileo* between the orbits of Io and Callisto (Krivov *et al.* 2002a). Similarly, ejecta from outer irregular moons could explain many of the *Galileo* detections in the outermost part of the jovian system (Krivov *et al.* 2002b). In the discussion that follows, we will confine our consideration to this mechanism because the first two mechanisms cannot explain the prograde populations between the Galilean satellites and do not explain any detections in the outer jovian satellite region.

The forces governing circumjovian dust described in Section 10.4.2 also govern larger grains; only the source and production mechanisms differ. Dynamics of sub-micron-sized particles, especially those ejected from Europa, is dominated by the Lorentz force. Dynamics of larger, micron-sized motes, especially those lost by Ganymede and Callisto, is controlled by two forces of comparable strength—the radiation pressure and the Lorentz force. The dynamics described in Section 10.4.2 now becomes more complex. Although the semimajor axis does not experience secular changes, orbital eccentricities and argument of pericenter evolve in a complicated way. The problem was studied both analytically and numerically (Hamilton and Krivov 1996, Krivov *et al.* 2002a). As the orbital inclinations have typically moderate values on the order of ten degrees, the dust ring formed by the particles is shifted azimuthally towards the Sun and is relatively flat.

The dynamics of all sizes of dusty ejecta from the Galilean satellites, is to some extent altered by another perturbing force—the satellite gravity. Its effects are particularly important during occasional close encounters of the dust particles with the moons, which may modify some individual orbits drastically. The net effect of the satellite gravity for a large ensemble of grains is a moderate radial and vertical broadening of the cloud.

An important question is: what are the main sinks of dust ejected from the Galilean satellites and what are the grains' typical lifetimes? Numerical simulations (Krivov *et al.* 2002a) show that the major loss mechanisms are grains re-impacting on to a parent moon (Io's and Europa's grains), collisions with a parent or another Galilean moon (dust from Ganymede), collisions with Jupiter or escapes from the jovian system (Callisto's dust). The typical lifetime is $\sim 10^2$ years, or $\sim 10^3$ to 10^4 revolutions about Jupiter, although the lifetimes of individual grains differ considerably—from less than a year to a few hundred years. Much longer survival times can be ruled out, being limited by other mech-

anisms: plasma sputtering and micrometeoroidal bombardment (Burns *et al.* 1984), surface erosion (Johnson *et al.* 1983), and even sublimation due to the heating by the radiation. The timescales involved make slow-acting mechanisms, such as the Poynting–Robertson effect or plasma drag, unimportant.

To model the steady-state spatial distribution of dust ejected from the three outer Galilean moons, Krivov *et al.* (2002a) launched test particles with the radius of 1 μm (close to the estimated DDS detection threshold) from surfaces of Europa, Ganymede and Callisto and obtain their spatial number density distribution (in arbitrary normalization). Finally, for the three source moons, they estimate steady-state numbers N of grains from the expected production rate (see Section 10.5.2) and grain lifetime. These numbers were applied to convert the arbitrary normalized spatial distribution of dust to the absolute number density of micron-sized grains at various distances from Jupiter. Figure 10.20 depicts the resulting number density profile. The profile derived from the *Galileo* measurements is overplotted, showing a good agreement with the model results. The number density has a maximum of $\sim 10^3 \text{ km}^{-3}$ near the orbit of Europa and gently decreases outward towards Jupiter, diminishing to a nearly-one order of magnitude smaller value at Callisto's orbit. Between the orbits of Europa and Ganymede the overwhelming majority of grains is supplied by Europa. Farther out, the Ganymede grains are the largest contribution. The Callisto particles are a minor part of dust everywhere in the ring.

We now consider the most distant region of the jovian system, from about 50 R_J outward. In this region, 70 tiny moons orbit the planet in prograde and 46 in retrograde orbits. These moons are expected to act as sources of dust through the same impact ejection mechanism, though the production mechanism is similar to the case of the Galilean moons, the subsequent dynamics of the dust ejecta is different here. As this region is located essentially outside the jovian magnetosphere, two dominant forces on the ejecta are solar tidal gravity and radiation pressure (Figure 10.10). An analytic and numerical study of the ejecta dynamics (Krivov *et al.* 2002b) shows that micron-sized particles from both satellite families would stay in bound orbits for typically $\sim 10^5$ yr. The main loss mechanism for these grains is the Poynting–Robertson drag that gradually decelerates the particles to the inner jovian system. On the other hand, smaller grains are usually lost on timescales of years.

Different-sized ejecta remain confined to spherical clouds embracing the orbits of the parent moons, with appreciable asymmetries created by the radiation pressure and solar gravity perturbations. The cloud formed by the ejecta from the retrograde moons is offset toward the Sun, whereas the cloud of the prograde ejecta is shifted in the opposite direction. In both cases, the orbital inclinations are pumped up by the perturbing forces to considerable values. For instance, grains from both satellite families with radii above 1 μm can reach polar orbits. Therefore, the outer satellite ejecta fill in a huge spatial volume—an effect that would considerably reduce the expected number densities of dust in the outskirts of the jovian system. Nevertheless, very long lifetimes of these grains, to a large extent, compensate this effect. As a result, the outer satellites are believed to sustain number densities of $\sim 10 \text{ km}^{-3}$, exceeding by a

of magnitude the interplanetary and interstellar background (Krivov *et al.* 2002b).

GOSSAMER RINGS

In about 3.1 R_J from Jupiter lies the region of Jupiter's inner ring system, which consists of three components: the main ring, the halo and the tenuous gossamer rings. The dust densities are so large that dust investigations can be performed with remote sensing techniques. The vertical extension and density profiles of the rings imply that a significant fraction if not all of the dust forming the rings is impact-ejecta derived from the inner moons Adrastea and Thebe (in the case of the main ring), and Amalthea and Europa (in the case of the gossamer rings (Ockert-Bell *et al.* 1999, Burns *et al.* 1999)). The orbits of these satellites are embedded in the ring system. The fraction of debris escaping the ring system is a steeply decreasing function of satellite mass, so that despite their reduced cross sections, small moons can be better sources of dust than large ones. For a detailed discussion of the jovian ring system the reader is referred to section 11.

In November 2002, *Galileo* traversed the gossamer ring system and passed by Amalthea. High-resolution dust data were obtained down to 2.33 R_J , i.e., just inside of Amalthea's orbit. Thus, in situ data were recorded in all three ring structures identified in *Galileo* and ground-based images (Ockert-Bell *et al.* 1999, De Pater *et al.* 1999, Burns *et al.* 1999). Several thousand dust impacts were counted in the ring system (Burns *et al.* 2003c). Our as yet preliminary analysis of impact particle sizes in the sub-micron and micron range. The distributions appear similar in the Thebe ring and the inner outer extension, whereas in the Amalthea ring it is different. Dust number densities are about 10^{-3} – 10^{-4} m^{-3} . The dust measurements allow for the first time to compare in situ measurements with optical imaging. Our preliminary analysis implies that small grains dominate the number density whereas larger particles contribute most to the optical depth. The in situ dust studies can improve our understanding of the forces dominating dust dynamics in the rings and the significance of small moons as sources of dust.

CONCLUSIONS AND OUTLOOK

The jovian dust streams discovered by *Ulysses* demonstrate that dust may become an intimate player in magnetospheric processes. We are still at the beginning of our understanding of these interrelations but the importance of dust is becoming evident. The dust streams monitor the volcanic plume activity on Io in a way that is not accomplished yet by any other observational method. Only a few images from the *Voyager* and *Galileo* spacecraft have shown the plumes.

Electromagnetically coupled dust grains are probes of the plasma environment in the Io torus, where they acquire their initial charge before they are emitted from the jovian magnetosphere by Jupiter's magnetosphere. Dust stream particles observed at different times originate from different portions of the Io torus. Therefore, observations tracing back to different local times in the Io torus reveal local time variations

in the torus that are predicted by theory. Dust stream particles are a promising new diagnostic tool to characterize the average properties of the jovian magnetosphere and they serve as carriers of information about the chemical composition of Io's volcanic plumes. In February 2004, *Ulysses* will fly by Jupiter within a distance of 0.8 AU. Additional dust stream measurements in interplanetary space at high jovigraphic latitudes will be beneficial to test our understanding of this new phenomenon.

Studies of the motion of charged dust particles connect a number of observations that are often thought to be unrelated. For example, images taken through filters at various phase angles provide data on the spatial and size distribution of the dust particles, in situ dust measurements provide data on their mass and the velocity vector. Since it is often the environment of the fields and particles that uniquely shapes the size, velocity and spatial distribution of the dust grains, images and in situ dust measurements can be used to test our models of the plasma environment.

The *Galileo* dust measurements close to the Galilean moons are the first successful in situ detection of satellite ejecta in the vicinity of a source moon. All celestial bodies without gaseous atmospheres (asteroids and planetary satellites of all sizes) should be surrounded by an ejecta dust cloud. Spacecraft measurements near satellites, i.e., very close to the sources of dust, are of primary importance to gain more insight into the properties of satellite surfaces and the dusty rings these moons maintain. This is especially important for the *Cassini* mission to the saturnian system. The *Cassini* dust instrument will obtain dust measurements during its flybys of the saturnian moons. Enceladus supplies material to the huge E ring (Hamilton and Burns 1994). Hyperion is believed to be a source of icy ejecta, which arrives at Titan, possibly affecting the chemistry of its atmosphere (Banaszkiewicz and Krivov 1997, Krivov and Banaszkiewicz 2001). Finally, Phoebe emits dust which may be deposited on the leading side of Iapetus, producing its observed brightness asymmetry (Burns *et al.* 1996). Since the *Cassini* dust instrument will measure the chemical composition of the grains, the surface properties of the source moons can be investigated remotely.

The *Galileo* dust measurements at the Galilean moons can be considered as unique natural impact experiments. They complement laboratory experiments in an astrophysically relevant environment. Laboratory impact experiments have significant deficiencies in many respects; in the speeds of the projectiles, and the mass and speed ranges in which ejecta particles can be observed. Furthermore, there is the question of the astrophysical relevance of the materials used. Although far from being perfect impact experiments, the *Galileo* results offer two extremely important improvements over laboratory experiments: (1) the projectile and target materials and projectile speeds are astrophysically relevant, and (2) the masses and speeds of the ejecta particles can be determined in an important region of parameter space (micron sizes and kms^{-1} speeds).

In situ dust measurements provide information about the physical properties of the dust environment not accessible with imaging techniques. The passage of *Galileo* through the gossamer rings in November 2002 provided the first ever opportunity for in situ studies of this dense dusty planetary ring. Analysis of this data is ongoing at the time of this

writing. They will eventually allow for comparative studies of a dusty ring with both in situ and remote sensing techniques for the first time. This can vastly improve our picture of grain dynamics in the gossamer ring, a necessary step in deriving a full understanding of the dust dynamics throughout the jovian magnetosphere. Comparative studies of ejecta from the large Galilean moons, and from the smaller ones embedded in the gossamer rings, will provide information about the ejection process over a large range in speed not accessible in the laboratory. Since all dusty planetary rings in our solar system are most likely dominated by impact ejecta, studies of Jupiter's gossamer ring provide valuable information not only about the mechanism feeding this ring system but also about the processes that govern planetary rings in general. Studies of the jovian ring by *Galileo* and of the saturnian ring by *Cassini* will lead to a vastly improved understanding of the formation and evolution of dusty planetary rings.

The *Galileo* dust measurements have raised a number of new questions about jovian dust, which are also related to the *Cassini* measurements at Saturn. They can be summarized as follows:

(1) A self-consistent model for the dynamics and evolution of the various jovian dust populations (cf. Table 10.1) including all relevant sources and sinks is still pending. Apart from deriving a coherent picture for the physics of jovian dust, one could "fly" a dust detector through such a model and make predictions for future spacecraft measurements.

(2) Our models describe the basic physics and dynamics of the jovian dust streams very well, however, the detailed connection between the measurements and Io's plume activity is not yet understood. This is also closely connected to the plasma conditions in the Io torus. The dust particles serve as probes of the plasma and fields environment in the torus. Comparative studies of the torus and the dust streams may help solve this problem.

(3) Studies of the gossamer ring are presently confined to remote imaging techniques. In situ *Galileo* measurements can better constrain the plasma conditions, grain properties and grain dynamics in the ring region. Together with a better understanding of the importance of moonlets embedded in the ring as sources and sinks of dust this can lead to a self-consistent picture for the formation and evolution of dust planetary rings in general.

(4) The *Galileo* dust measurements at Jupiter will be the most comprehensive and homogeneous data set of a planetary dust environment for many years to come. We are just beginning to recognize and to understand long-term variabilities in the data set. Temporal and spatial variations may show up, e.g., due to asymmetries in the circumsatellite dust clouds or dust ejected into the jovian system during the break-up of Comet Shoemaker-Levy 9 in 1992.

Acknowledgements. The authors are gratefully indebted to Hugo Fechtig, Eberhard Grün and the numerous *Galileo* and *Ulysses* co-investigators. Without their continuous efforts over the years the *Galileo* and *Ulysses* dust investigations would not have become reality. This research has been supported by the German Bundesministerium für Bildung und Forschung through Deutsches Zentrum für Luft-

und Raumfahrt e.V. (DLR, grants 50 QJ 9503 3 50 OH 0003). Support by Deutsche Forschungsgemeinschaft (DFG) and Max-Planck-Institut für Kernphysik (MPI) also gratefully acknowledged. We wish to thank the *G* and *Ulysses* projects at JPL and ESTEC for effective successful mission operations.

REFERENCES

- Acuña, M. and N. Ness, The complex main magnetic field of Jupiter, *J. Geophys. Res.* **81**, 2917–2922, 1976.
- Bagenal, F., Torus-magnetosphere coupling, in *Time-variable Phenomena in the Jovian System*, M. J. S. Belton, J. West, J. Rahe (eds), NASA-SP-494, 1989.
- Bagenal, F., Empirical model of the Io plasma torus: Voyager measurements, *J. Geophys. Res.* **99**, 11 043–11 062, 1994.
- Baguhl, M., E. Grün, G. Linkert, D. Linkert, and N. Sidiropoulos, Identification of "small" dust impacts in the *Ulysses* dust detector data, *Planet. Space Sci.* **41**, 1085–1098, 1993.
- Banaszkiewicz, M. and A. V. Krivov, Hyperion as a dust source in the saturnian system, *Icarus* **129**, 289–303, 1997.
- Burns, J. A., P. L. Lamy, and S. Soter, Radiation forces on dust particles in the solar system, *Icarus* **40**, 1–48, 1979.
- Burns, J. A., M. R. Showalter, and G. E. Morfill, The ethereal rings of Jupiter and Saturn, in *Planetary Rings*, R. Green and A. Brahic (eds), University of Arizona Press, pp. 200–218, 1984.
- Burns, J. A., D. P. Hamilton, F. Mignard, and S. Soter, The formation of Iapetus by Phoebe dust, in *Physics, Chemistry and Dynamics of Interplanetary Dust*, B. A. S. Gustafson, M. S. Hanner, eds, vol. 104, pp. 179–182, ASP, Kluwer, 1993.
- Burns, J. A., M. R. Showalter, D. P. Hamilton, P. D. Nicholson, I. de Pater, M. E. Ockert-Bell, and P. C. Thomas, The formation of Jupiter's faint rings, *Science* **284**, 1146–1150, 1999.
- Burns, J. A., D. P. Hamilton, and M. R. Showalter, Dusty Iapetus and Circumplanetary Dust: Observations and Simple Physics, in *Interplanetary Dust*, E. Grün, B. A. S. Gustafson, H. Fechtig, and H. Fechtig, eds, pp. 641–725, Springer-Verlag, 2001.
- Chow, V. W., D. A. Mendis, and M. Rosenberg, Role of grain-grain and particle velocity distribution in secondary electron emission in space plasmas, *J. Geophys. Res.* **98**, 19 065–19 073, 1993.
- Collins, S. A., Spatial color variations in the volcanic plume of Loki on Io, *J. Geophys. Res.* **86**, 8621–8626, 1981.
- Colwell, J. E., A general formulation for the distribution of impacts and ejecta from small planetary satellites, *Icarus* **2**, 536–548, 1993.
- Colwell, J. E. and M. Horányi, Magnetospheric effects on micrometeoroid fluxes, *J. Geophys. Res.* **101**, 2169–2175, 1996.
- Colwell, J. E., M. Horányi, and E. Grün, Jupiter's exogenic ring, *J. Geophys. Res.* **103**, 20 023–20 030, 1998a.
- Colwell, J. E., M. Horányi, and E. Grün, Capture of interplanetary and interstellar dust by the jovian magnetosphere, *Science* **280**, 88–91, 1998b.
- Connerney, J. E. P., The magnetic fields of the outer planets, *J. Geophys. Res.* **98**, 18 659–18 679, 1993.
- Connerney, J. E. P., M. H. Acuña, N. F. Ness, and T. Satoh, Models of Jupiter's magnetic field constrained by the Io tube footprint, *J. Geophys. Res.* **103**, 11 929–11 940, 1998.
- De Pater, I., M. R. Showalter, J. A. Burns, P. D. Nicholson, M. Liu, D. P. Hamilton, and J. R. Graham, Keck infrared observations of Jupiter's Ring System near Earth's 1997 ring plane crossing, *Icarus* **138**, 214–223, 1999.
- Fechtig, H., C. Leinert, and O. E. Berg, Historical Perspective on Interplanetary Dust, E. Grün, B. A. S. Gustafson, S. F. J.

- mott, and H. Fechtig, eds, pp. 1–55, Springer Verlag, Berlin Heidelberg New York, 2001.
- Fillius, R. W., C. E. McIlwain, and A. Mogro-Campero, Radiation belts of Jupiter: A second look, *Science* **188**, 465–467, 1975.
- Frank, L. A., K. L. Ackerson, J. A. Lee, M. R. English, and G. L. Pickett, The Plasma Instrumentation for the *Galileo* mission, *Space Science Reviews* **60**, 283–307, 1992.
- Frisch, W., Hypervelocity impact experiments with water ice targets, in *Hypervelocity Impact Symposium*, pp. 7–14, 1992.
- Geissler, P. E., A. McEwen, C. Phillips, L. Kesthelyi, and J. Spencer, Surface Changes on Io during the *Galileo* Mission, *Icarus* in press, 2003.
- Graps, A. L., *Io revealed in the jovian dust streams*, Ph.D. thesis, Ruprecht-Karls-Universität Heidelberg, 2001.
- Graps, A. L., E. Grün, H. Svedhem, H. Krüger, M. Horányi, A. Heck, and S. Lammers, Io as a source of the jovian dust streams, *Nature* **405**, 48–50, 2000.
- Graps, A. L., E. Grün, H. Krüger, M. Horányi, and H. Svedhem, Io revealed in the jovian dust streams, in *Proceedings of the Meteoroids 2001 Conference*, ESA SP-495, pp. 601–608, 2001.
- Grün, E., H. Fechtig, M. S. Hanner, J. Kissel, B. A. Lindblad, D. Linkert, D. Maas, G. E. Morfill, and H. A. Zook, The *Galileo* dust detector, *Space Sci. Rev.* **60**, 317–340, 1992a.
- Grün, E., H. Fechtig, J. Kissel, D. Linkert, D. Maas, J. A. M. McDonnell, G. E. Morfill, G. H. Schwehm, H. A. Zook, and R. H. Giese, The *Ulysses* dust experiment, *A&AS* **92**, 411–423, 1992b.
- Grün, E., H. A. Zook, M. Baguhl, A. Balogh, S. J. Bame, H. Fechtig, R. Forsyth, M. S. Hanner, M. Horányi, J. Kissel, B. A. Lindblad, D. Linkert, G. Linkert, I. Mann, J. A. M. McDonnell, G. E. Morfill, J. L. Phillips, C. Polanskey, G. H. Schwehm, N. Siddique, P. Staubach, J. Svestka, and A. Taylor, Discovery of jovian dust streams and interstellar grains by the *Ulysses* spacecraft, *Nature* **362**, 428–430, 1993.
- Grün, E., M. Baguhl, N. Divine, H. Fechtig, D. P. Hamilton, M. S. Hanner, J. Kissel, B. A. Lindblad, D. Linkert, G. Linkert, I. Mann, J. A. M. McDonnell, G. E. Morfill, C. Polanskey, R. Riemann, G. H. Schwehm, N. Siddique, P. Staubach, and H. A. Zook, Three years of *Galileo* dust data, *Planet. Space Sci.* **43**, 953–969, 1995a.
- Grün, E., M. Baguhl, N. Divine, H. Fechtig, D. P. Hamilton, M. S. Hanner, J. Kissel, B. A. Lindblad, D. Linkert, G. Linkert, I. Mann, J. A. M. McDonnell, G. E. Morfill, C. Polanskey, R. Riemann, G. H. Schwehm, N. Siddique, P. Staubach, and H. A. Zook, Two years of *Ulysses* dust data, *Planet. Space Sci.* **43**, 971–999, 1995b.
- Grün, E., M. Baguhl, D. P. Hamilton, J. Kissel, D. Linkert, G. Linkert, and R. Riemann, Reduction of *Galileo* and *Ulysses* dust data, *Planet. Space Sci.* **43**, 941–951, 1995c.
- Grün, E., M. Baguhl, D. P. Hamilton, R. Riemann, H. A. Zook, S. F. Dermott, H. Fechtig, B. A. Gustafson, M. S. Hanner, M. Horányi, K. K. Khurana, J. Kissel, M. Kivelson, B. A. Lindblad, D. Linkert, G. Linkert, I. Mann, J. A. M. McDonnell, G. E. Morfill, C. Polanskey, G. H. Schwehm, and R. Srama, Constraints from *Galileo* observations on the origin of jovian dust streams, *Nature* **381**, 395–398, 1996a.
- Grün, E., D. P. Hamilton, R. Riemann, S. F. Dermott, H. Fechtig, B. A. Gustafson, M. S. Hanner, A. Heck, M. Horányi, J. Kissel, M. Kivelson, H. Krüger, B. A. Lindblad, D. Linkert, G. Linkert, I. Mann, J. A. M. McDonnell, G. E. Morfill, C. Polanskey, G. H. Schwehm, R. Srama, and H. A. Zook, Dust measurements during *Galileo's* approach to Jupiter and Io encounter, *Science* **274**, 399–401, 1996b.
- Grün, E., P. Krüger, S. F. Dermott, H. Fechtig, A. L. Graps, B. A. Gustafson, D. P. Hamilton, A. Heck, M. Horányi, J. Kissel, B. A. Lindblad, D. Linkert, G. Linkert, I. Mann, J. A. M. McDonnell, G. E. Morfill, C. Polanskey, G. H. Schwehm, R. Srama, and H. A. Zook, Dust measurements in the jovian magnetosphere, *Geophys. Res. Lett.* **24**, 2171–2174, 1997.
- Grün, E., H. Krüger, A. Graps, D. P. Hamilton, A. Heck, G. Linkert, H. Zook, S. F. Dermott, H. Fechtig, B. Gustafson, M. Hanner, M. Horányi, J. Kissel, B. Lindblad, G. Linkert, I. Mann, J. A. M. McDonnell, G. E. Morfill, C. Polanskey, G. H. Schwehm, and R. Srama, *Galileo* observes electromagnetically coupled dust in the jovian magnetosphere, *J. Geophys. Res.* **103**, 20011–20022, 1998.
- Grün, E., H. Krüger, and M. Landgraf, Cosmic Dust, in *The heliosphere at solar minimum: The Ulysses perspective*, A. Balogh, R. Marsden, and E. Smith, eds, pp. 373–404, Springer Praxis, 2001.
- Hamilton, D. P., Motion of dust in a planetary magnetosphere—Orbit-averaged equations for oblateness, electromagnetic, and radiation forces with application to Saturn's E ring, *Icarus* **101**, 2, 244–264, 1993.
- Hamilton, D. P. and J. A. Burns, Ejection of dust from Jupiter's gossamer ring, *Nature* **364**, 695–699, 1993.
- Hamilton, D. P. and A. V. Krivov, Circumplanetary dust dynamics: Effects of solar gravity, radiation pressure, planetary oblateness, and electromagnetism, *Icarus* **123**, 503–523, 1996.
- Hamilton, D. P. and Burns, J. A., Origin of Saturn's E ring: Self-sustained – naturally, *Science* **264**, 550–553, 1994.
- Hartmann, W. K., Impact experiments: 1. Ejecta velocity distributions and related results from regolith targets, *Icarus* **63**, 69–98, 1985.
- Heck, A., *Modellierung und Analyse der von der Raumsonde Galileo im Jupitersystem vorgefundenen Mikrometeoroiden-Populationen*, Ph.D. thesis, Ruprecht-Karls-Universität Heidelberg, 1998.
- Horányi, M., New jovian ring?, *Geophys. Res. Lett.* **21**, 1039–1042, 1994.
- Horányi, M., Charged dust dynamics in the solar system, *Ann. Rev. Astron. Astrophys.* **34**, 383–418, 1996.
- Horányi, M., Unusual dynamics of circumplanetary dust, in *Completing the Inventory of the solar system*, T. W. Rettig and J. M. Hahn, eds, 1996.
- Horányi, M., G. E. Morfill, and E. Grün, Mechanism for the acceleration and ejection of dust grains from Jupiter's magnetosphere, *Nature* **363**, 144–146, 1993a.
- Horányi, M., G. E. Morfill, and E. Grün, The dusty ballerina skirt of Jupiter, *J. Geophys. Res.* **98**, 21245–21251, 1993b.
- Horányi, M., E. Grün, and A. Heck, Modeling the *Galileo* dust measurements at Jupiter, *Geophys. Res. Lett.* **24**, 2175–2178, 1997.
- Humes, D. H., J. M. Alvarez, R. L. O'Neal, and W. H. Kinard, The interplanetary and near-Jupiter meteoroid environment, *J. Geophys. Res.* **79**, 3677–3684, 1974.
- Ip, W. H., The dust halo of Io, *Geophys. Res. Lett.* **24**, 3671–3674, 1996.
- Johnson, R. E., J. W. Boring, C. T. Reimann, L. A. Barton, J. W. Sieveka, J. W. Garrett, K. R. Farmer, W. L. Brown, and L. J. Lanzerotti, Plasma ion-induced molecular ejection on the Galilean satellites: Energies of ejected molecules, *Geophys. Res. Lett.* **10**, 892–895, 1983.
- Johnson, T. V., G. E. Morfill, and E. Grün, Dust in Jupiter's magnetosphere: An Io source, *Geophys. Res. Lett.* **7**, 305–308, 1980.
- Keszthelyi, L., A. S. McEwen, C. B. Phillips, M. Milazzo, P. Geissler, E. P. Turtle, J. Radebaugh, D. A. Williams, D. P. Simonelli, H. H. Breneman, K. P. Klaasen, G. Levanas, and T. Denk, and the *Galileo* SSI Team, Imaging of volcanic activity on Jupiter's moon Io by *Galileo* during the *Galileo* Europa mission and the *Galileo* millennium mission, *J. Geophys. Res.* **106**, 33025–33052, 2001.

- Kivelson, M. G., K. K. Khurana, J. D. Means, C. T. Russell, and R. C. Snare, The *Galileo* magnetic field investigation, *Space Sci. Rev.* **60**, 357–383, 1992.
- Krivov, A. V. and H. Banaszekiewicz, Unusual origin, evolution and fate of icy ejecta from Hyperion, *Planet. Space Sci.* **49**, 1265–1279, 2001.
- Krivov, A. V., H. Krüger, E. Grün, K.-U. Thiessenhusen, and D. P. Hamilton, A tenuous dust ring of Jupiter formed by escaping ejecta from the Galilean satellites, *J. Geophys. Res.* **107**, E1, 10.1029/2000JE001434, 2002a.
- Krivov, A. V., I. Wardinski, F. Spahn, H. Krüger, and E. Grün, Dust on the outskirts of the jovian system, *Icarus* **157**, 436–455, 2002b.
- Krivov, A. V., M. Sremčević, F. Spahn, V. V. Dikarev, and K. V. Kholshchevnikov, Impact-generated dust clouds around planetary satellites: Spherically-symmetric case, *Planet. Space Sci.* **51**, 251–269, 2003.
- Krüger, H. and E. Grün, Dust en-route to Jupiter and the Galilean satellites, in *Dust in the Solar System and in Other Planetary Systems*, S. F. Green, I. Williams, T. McDonnell and N. McBride (eds), IAU/COSPAR 11, pp. 144–159, 2002.
- Krüger, H., E. Grün, A. L. Graps, and S. Lammers, Observations of electromagnetically coupled dust in the jovian magnetosphere, in *Proceedings of the VII International Conference on Plasma Astrophysics and Space Physics*, J. Büchner, I. Axford, E. Marsch and V. Vasyliunas (eds), vol. 264, pp. 247–256, 1999a.
- Krüger, H., E. Grün, D. P. Hamilton, M. Baguhl, S. F. Dermott, H. Fechtig, B. A. Gustafson, M. S. Hanner, M. Horányi, J. Kissel, B. A. Lindblad, D. Linkert, G. Linkert, I. Mann, J. A. M. McDonnell, G. E. Morfill, C. Polanskey, R. Riemann, G. H. Schwehm, R. Srama, and H. A. Zook, Three years of *Galileo* dust data: II. 1993 to 1995, *Planet. Space Sci.* **47**, 85–106, 1999b.
- Krüger, H., E. Grün, A. Heck, and S. Lammers, Analysis of the sensor characteristics of the *Galileo* dust detector with collimated jovian dust stream particles, *Planet. Space Sci.* **47**, 1015–1028, 1999c.
- Krüger, H., E. Grün, M. Landgraf, M. Baguhl, S. F. Dermott, H. Fechtig, B. A. Gustafson, D. P. Hamilton, M. S. Hanner, M. Horányi, J. Kissel, B. Lindblad, D. Linkert, G. Linkert, I. Mann, J. A. M. McDonnell, G. E. Morfill, C. Polanskey, G. H. Schwehm, R. Srama, and H. A. Zook, Three years of *Ulysses* dust data: 1993 to 1995, *Planet. Space Sci.* **47**, 363–383, 1999d.
- Krüger, H., A. V. Krivov, D. P. Hamilton, and E. Grün, Detection of an impact-generated dust cloud around Ganymede, *Nature* **399**, 558–560, 1999e.
- Krüger, H., A. V. Krivov, and E. Grün, A dust cloud of Ganymede maintained by hypervelocity impacts of interplanetary micrometeoroids, *Planet. Space Sci.* **48**, 1457–1471, 2000.
- Krüger, H., E. Grün, A. L. Graps, D. L. Bindschadler, S. F. Dermott, H. Fechtig, B. A. Gustafson, D. P. Hamilton, M. S. Hanner, M. Horányi, J. Kissel, B. Lindblad, D. Linkert, G. Linkert, I. Mann, J. A. M. McDonnell, G. E. Morfill, C. Polanskey, G. H. Schwehm, R. Srama, and H. A. Zook, One year of *Galileo* dust data: 1996, *Planet. Space Sci.* **49**, 1285–1301, 2001a.
- Krüger, H., E. Grün, M. Landgraf, S. F. Dermott, H. Fechtig, B. A. Gustafson, D. P. Hamilton, M. S. Hanner, M. Horányi, J. Kissel, B. Lindblad, D. Linkert, G. Linkert, I. Mann, J. A. M. McDonnell, G. E. Morfill, C. Polanskey, G. H. Schwehm, R. Srama, and H. A. Zook, Four years of *Ulysses* dust data: 1996 to 1999, *Planet. Space Sci.* **49**, 1303–1324, 2001b.
- Krüger, H., P. Geissler, M. Horányi, A. L. Graps, S. Kempf, R. Srama, G. Moragas-Klostermeyer, R. Moissl, T. V. Johnson, and E. Grün, Jovian dust streams: A monitor of Io's volcanic plume activity, *Geophys. Res. Lett.* **30**(2), 2101, 2003a.
- Krüger, H., E. Grün, D. Linkert, G. Linkert, and R. Moissl, Long-term operation of the *Galileo* and *Ulysses* dust instruments, *Planet. Space Sci.* submitted, 2003b.
- Krüger, H., E. Grün, the *Galileo*, and *Ulysses* dust science teams, *Galileo* dust measurements in Jupiter's gossamer ring, *Icarus* in preparation, 2003c.
- Krüger, H., M. Horányi, and E. Grün, Jovian dust streams: Probes of the Io plasma torus, *Geophys. Res. Lett.* **30**(2), 1058, 2003d.
- Krüger, H., A. V. Krivov, M. Sremčević, and E. Grün, *Galileo* measurements of impact-generated dust clouds surrounding the Galilean satellites, *Icarus* **164**, 170–187, 2003e.
- Maravilla, D., K. R. Flammer, and D. A. Mendis, On the injection of fine dust from the jovian magnetosphere, *ApJ* **438**, 968–974, 1995.
- McEwen, A. S., L. Keszthelyi, P. Geissler, D. P. Simonelli, M. H. Carr, T. V. Johnson, K. P. Klaasen, H. H. Breneman, T. J. Jones, J. M. Kaufman, K. P. Magee, D. A. Senske, M. J. S. Belton, and G. Schubert, Active volcanism on Io as seen by *Galileo* SSI, *Icarus* **135**, 181–219, 1998.
- Morfill, G. E., E. Grün, and T. V. Johnson, Dust in Jupiter's magnetosphere: Physical processes, *Planet. Space Sci.* **28**, 1087–1100, 1980.
- Ockert-Bell, M. E., J. A. Burns, I. J. Daubar, P. C. Thomas, J. Veverka, M. J. S. Belton, and K. P. Klaasen, The structure of Jupiter's ring system as revealed by the *Galileo* imaging experiment, *Icarus* **138**, 188–213, 1999.
- Scargle, J. D., Studies in astronomical time series: II. Statistical aspects of spectral analysis of unevenly spaced data, *A J* **263**, 835–853, 1982.
- Spencer, J. R., P. Sartoretti, G. E. Bellester, A. S. McEwen, J. T. Clarke, and M. A. McGrath, The Pele plume (Io): Observations with the Hubble Space Telescope, *Geophys. Res. Lett.* **24**, no. 20, 2471–2474, 1997.
- Spencer, J. R., K. L. Jessup, M. A. McGrath, G. E. Ballester, and R. Yelle, Discovery of gaseous S₂ in Io's Pele plume, *Science* **288**, 1208–1210, 2000.
- Srama, R., J. G. Bradley, E. Grün, T. J. Ahrens, S. Auer, M. Cruise, H. Fechtig, A. L. Graps, O. Havnes, A. Heck, S. Helfert, E. Igenbergs, E. K. Jeßberger, T. V. Johnson, S. Kempf, H. Krüger, P. Lamy, M. Landgraf, D. Linkert, F. Lura, J. A. M. McDonnell, D. Möhlmann, G. E. Morfill, G. H. Schwehm, M. Stübig, J. Vestka, A. J. Tuzzolino, R. Wäsch, and H. A. Zook, The *Cassini* Cosmic Dust Analyzer, *Space Sci. Rev.* submitted, 2004.
- Sremčević, M., A. V. Krivov, and F. Spahn, Impact-generated dust clouds around planetary satellites: Asymmetry effects, *Planet. Space Sci.* **51**, 455–471, 2003.
- Stöffler, D., D. E. Gault, J. Wedekind, and R. Polkowski, Experimental hypervelocity impact into quartz sand: Distribution and shock metamorphism of ejecta, *J. Geophys. Res.* **80**, 4042–4077, 1975.
- Thiessenhusen, K.-U., H. Krüger, F. Spahn, and E. Grün, Dust grains around Jupiter: The observations of the *Galileo* Dust Detector, *Icarus* **144**, 89–98, 2000.
- Whipple, E. C., Potentials of surfaces in space, *Rep. Prog. Phys.* **44**, 1197–1250, 1981.
- Whipple, F. L., The cometary nucleus: current concepts, *Astron. Astrophys.* **187**, 852–858, 1987.
- Williams, D. J., R. W. McEntire, S. Jaskulek, and B. Wilken, The *Galileo* Energetic Particles Detector, *Space Sci. Rev.* **60**, 385–412, 1992.
- Zook, H. A., E. Grün, M. Baguhl, D. P. Hamilton, G. Linkert, D. Linkert, J.-C. Liou, R. Forsyth, and J. L. Phillips, Solar wind magnetic field bending of jovian dust trajectories, *Science* **274**, 1501–1503, 1996.